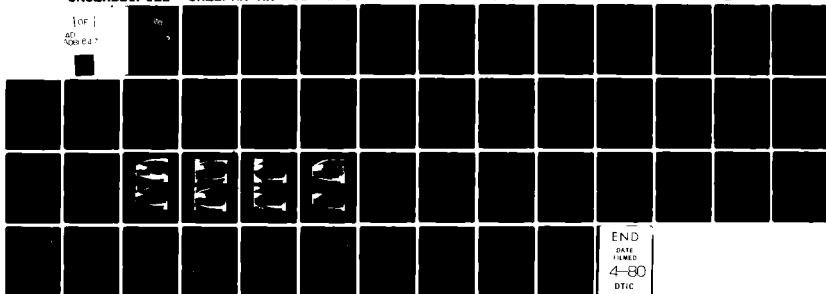


AD-A081 647 CALSPAN ADVANCED TECHNOLOGY CENTER BUFFALO NY AERODYN--ETC F/6 21/8  
ANALYSIS OF EXPERIMENTS ON THE EFFECTS OF JET PLUMES ON PRESSUR--ETC  
FEB 80 J P NENNI DAA829-77-C-0008  
UNCLASSIFIED CALSPAN-AA-4017-W-16 ARO-13797.1-E NL

1 of 1  
AD  
A081 647



AD A081647

ARO 13797.1-E  
(12)  
R

ANALYSIS OF EXPERIMENTS ON THE EFFECTS  
OF JET PLUMES ON PRESSURE DISTRIBUTION OVER  
A CYLINDRICAL AFTERBODY AT TRANSONIC SPEEDS

LEVEL

FINAL REPORT

J.P. Nenni

January 1980

DTIC  
SELECTED  
MAR 11 1980  
S C

Contract No.

DAAG29-77-C-0008

AROD Project No. 13797-E

CALSPAN ADVANCED TECHNOLOGY CENTER  
AERODYNAMIC RESEARCH DEPARTMENT  
BUFFALO, NEW YORK 14225

Approved for public release;  
distribution unlimited.

80 3 7 068

DDC FILE COPY

THE FINDINGS IN THIS REPORT ARE NOT TO BE  
CONSTRUED AS AN OFFICIAL DEPARTMENT OF  
THE ARMY POSITION, UNLESS SO DESIGNATED  
BY OTHER AUTHORIZED DOCUMENTS.

(18) AKO  
Unclassified

(19) 13797.1-E

SECURITY CLASSIFICATION OF THIS PAGE (When Data Entered)

REPORT DOCUMENTATION PAGE		READ INSTRUCTIONS BEFORE COMPLETING FORM
1. REPORT NUMBER 13797-E	2. GOVT ACCESSION NO.	3. RECIPIENT'S CATALOG NUMBER (9)
4. TITLE (and Subtitle) ANALYSIS OF EXPERIMENTS ON THE EFFECTS OF JET PLUMES ON PRESSURE DISTRIBUTION OVER A CYLINDRICAL AFTERBODY AT TRANSONIC SPEEDS.		5. DATE OF REPORT & PERIOD COVERED Final Technical Report
7. AUTHOR(s) (10) Joseph P. Nenni		6. PERFORMING ORG. REPORT NUMBER -AA-4017-W-16/
9. PERFORMING ORGANIZATION NAME AND ADDRESS CALSPAN ADVANCED TECHNOLOGY CENTER P.O. BOX 400 BUFFALO, NY 14225		8. CONTRACT OR GRANT NUMBER(s) (15) DAAG29-77-0008
11. CONTROLLING OFFICE NAME AND ADDRESS U.S. ARMY RESEARCH OFFICE P.O. BOX 12211 RESEARCH TRIANGLE PARK, NORTH CAROLINA 27709		10. PROGRAM ELEMENT, PROJECT, TASK AREA & WORK UNIT NUMBERS
14. MONITORING AGENCY NAME & ADDRESS (if different from Controlling Office) (12) 50		12. REPORT DATE (11) February 1980
		13. NUMBER OF PAGES 42
		15. SECURITY CLASS. (of this report) Unclassified
		15a. DECLASSIFICATION/DOWNGRADING SCHEDULE NA
16. DISTRIBUTION STATEMENT (of this Report)  Approved for public release; distribution unlimited.		
17. DISTRIBUTION STATEMENT (of the abstract entered in Block 20, if different from Report)  NA		
18. SUPPLEMENTARY NOTES  The findings in this report are not to be construed as an official Department of the Army position, unless so designated by other authorized documents.		
19. KEY WORDS (Continue on reverse side if necessary and identify by block number)  Jet plumes Transonic flow Afterbody pressures Jet modeling		
20. ABSTRACT (Continue on reverse side if necessary and identify by block number)  The objective of the present investigation was to obtain experimentally, the effects of various jet plume parameters on afterbody pressure distributions and to partially validate the Korst modeling procedure. Analysis of the experimental results and supplemental calculations made by the method of characteristics show that the approximate theory used by Korst, gives a good estimate		

DD FORM 1 JAN 73 1473

EDITION OF 1 NOV 65 IS OBSOLETE

Unclassified

SECURITY CLASSIFICATION OF THIS PAGE (When Data Entered)

391214

Unclassified

SECURITY CLASSIFICATION OF THIS PAGE(When Data Entered)

20. Abstract (continued)

of the plume shape for nozzle exit Mach numbers of 2.0 and below. For nozzle exit Mach numbers much in excess of 2.0, it appears desirable to include the effect of the nozzle wall boundary layer on plume shape.

In addition, afterbody pressure distributions produced by a series of nozzles designed to produce the same plume shape, but with different values of the plume pliability parameter, have been compared with results from a solid plume simulator. In general, the solid plume simulator produces results that agree with the nozzles with the higher values of the plume pliability parameter at zero degrees angle of attack. The correlation deteriorates significantly, however, at five degrees angle of attack.

Also, afterbody pressure distributions from model tests on the ZAP rocket motor are presented for future correlation with prototype results.

Unclassified

SECURITY CLASSIFICATION OF THIS PAGE(When Data Entered)

# FOREWORD

This work was performed for the U. S. Army Research Office, Research Triangle Park, North Carolina and the U. S. Army MIRADCOM, Redstone Arsenal, Alabama under contract number DAAG29-77-C-0008. The experimental portion of this program was performed in the 8-Foot Transonic Wind Tunnel Department of the Calspan Advanced Technology Center, and Mr. C. Reid of that department was overall program manager. The work reported here was performed in the Aerodynamic Research Department under the direction of Dr. Joseph P. Nenni. The author wishes to acknowledge Dr. J. Curtis and Mr. J. Moselle of the Aerodynamic Research Department for performing calculations of nozzle and plume flow fields with the PIP Code. Also, discussions with Drs. T. Falk and D. Boyer were helpful in assisting the author to interpret schlieren photos of the plumes.

Accession For	
NTIS GRA&I	<input checked="checked" type="checkbox"/>
DEC TAB	<input type="checkbox"/>
Unannounced	<input type="checkbox"/>
Justification	
By _____	
Distribution/	
Availability Codes	
Dist.	Avail and/or special
A	

## TABLE OF CONTENTS

<u>Section</u>	<u>Page</u>
I. INTRODUCTION .....	1
II. DESCRIPTION OF WIND TUNNEL TESTS .....	3
III. COMPARISON OF PLUME SHAPES .....	7
a) Discussion of the Calculation Procedure .....	7
b) Results of Calculations .....	9
c) Comparison with Schlieren Photos .....	9
d) Nozzle Pressure Distributions .....	10
IV. AFTERBODY PRESSURE DISTRIBUTIONS .....	11
a) Similar Plume Shape Models .....	11
b) Validation of the Korst Modeling Procedures .....	12
c) ZAP Models .....	13
V. CONCLUSIONS AND RECOMMENDATIONS .....	14

# LIST OF FIGURES

<u>Figure</u>		<u>Page</u>
1	Comparison of Calculated Plume Shapes, Nozzle NC .8 1.7 . . . . .	15
2	Comparison of Calculated Plume Shapes, Nozzle NC .8 2.0 . . . . .	16
3	Comparison of Calculated Plume Shapes, Nozzle NC .8 2.4 . . . . .	17
4	Comparison of Calculated Plume Shapes, Nozzle NC .8 2.7 . . . . .	18
5	Effect of Nozzle Starting Line Conditions on Plume Shape, Nozzle NC .8 1.7 with no Nozzle Boundary Layer. . . . .	19
6	Effect of Nozzle Starting Line Conditions on Plume Shape, Nozzle NC .8 2.7 with no Nozzle Boundary Layer. . . . .	20
7	Comparison of Korst Plume Shape with Experiment, Nozzle NC .8 1.7 . . . . .	21
8	Comparison of Korst Plume Shape with Experiment, Nozzle NC .8 2.0 . . . . .	22
9	Comparison of Korst Plume Shape with Experiment, Nozzle NC .8 2.4 . . . . .	23
10	Comparison of Korst Plume Shape with Experiment, Nozzle NC .8 2.7 . . . . .	24
11.	Nozzle Wall Pressure Distribution - Nozzle NC .8 1.7 . . . . .	25
12	Nozzle Wall Pressure Distribution - Nozzle NC .8 2.0 . . . . .	26
13	Nozzle Wall Pressure Distribution - Nozzle NC .8 2.4 . . . . .	27
14	Nozzle Wall Pressure Distribution - Nozzle NC .8 2.7 . . . . .	28
15	Comparison of Afterbody Pressure Distributions with Rocket Nozzles Operating at Design Values, $M_\infty = 0.4$ . . . . .	29

# LIST OF FIGURES (continued)

<u>Figure</u>		<u>Page</u>
16	Comparison of Afterbody Pressure Distribution with Rocket Nozzles Operating at Design Values $M_\infty = 0.7$ .....	30
17	Comparison of Afterbody Pressure Distribution with Rocket Nozzles Operating at Design Values $M_\infty = 0.9$ .....	31
18	Comparison of Afterbody Pressure Distribution with Rocket Nozzles Operating at Design Values $M_\infty = 1.001$ .....	32
19	Comparison of Afterbody Pressure Distribution with Rocket Nozzles Operating at Design Values $M_\infty = 1.1$ .....	33
20	Comparison of Afterbody Pressure Distributions with Rocket Nozzles Operating at Design Values $M_\infty = 1.25$ .....	34
21	Comparison of Afterbody Pressure Distribution for Solid Jet Simulator and Nozzle NC $\frac{.8}{2.7}$ at Design Pressure Ratio, $M_\infty = 0.9$ , $\alpha = -5^\circ$ .....	35
22	Effect of Nozzle Total Pressure to Base Pressure Ratio on Afterbody Pressure Distribution -NC $\frac{.8}{1.7}$ , $M_\infty = 0.4$ ....	36
23	Effect of Nozzle Total Pressure to Base Pressure Ratio on Afterbody Pressure Distribution -NC $\frac{.8}{1.7}$ , $M_\infty = 0.9$ ....	37
24	Effect of Nozzle Total Pressure to Base Pressure Ratio on Afterbody Pressure Distribution -NC $\frac{.8}{1.7}$ , $M_\infty = 1.25$ ...	38
25	Afterbody Pressure Distribution on Large ZAP Nozzle - NZ $\frac{.93}{1.76}$ .....	39
26	Afterbody Pressure Distribution on Small ZAP Nozzle - NZ $\frac{.8}{1.76}$ .....	40

## I. INTRODUCTION

The propulsive jet issuing from the base of a missile can have a significant influence upon the drag level and stability characteristics of the missile. Considerable capability<sup>1</sup> exists for analytically calculating axially symmetric afterbody-jet flows with supersonic external streams as long as boundary layer separation is not induced on the afterbody<sup>2</sup>. Similar capabilities are also now emerging for transonic external streams<sup>3</sup>. However, some of the most significant effects of the propulsive jet on the missile afterbody are associated with induced separation and angle of attack effects. Presently, these interesting phenomena can only be investigated experimentally.

Exact experimental simulation requires that a number of parameters be the same for the model and the prototype. The more important of these parameters are

- similar body geometry (internal & external)
- jet thermodynamic characteristics  
(chiefly the ratio of specific heats,  $\gamma$  )
- exit Mach Number
- ratio of jet total pressure to ambient static pressure.

It is difficult to simulate all of these parameters in a wind tunnel unless the wind tunnel is specially designed with a system to supply typical exhaust products of rocket engines. Such a facility has been designed in Sweden<sup>3</sup> with an elaborate supply system for the propulsive exhaust effluents. Clearly, the usefulness of existing wind tunnels could be greatly enhanced if a set of approximate scaling laws could be developed such that air or other commonly available gases could be used for the propulsive effluent. Korst<sup>4,5</sup> has been working on the development of such a set of approximate scaling laws for supersonic jets for some time. The basic tenet of Korst's modeling procedure is the requirement that the model and prototype should produce similar plume shapes in the immediate neighborhood of the nozzle exits when the nozzles are exhausting into quiescent air. This is accomplished by requiring the model and prototype nozzles to produce plumes with the same initial divergence angles and geometrically-scaled radii of curvature. These requirements on plume shape similarity are, however, not sufficient to close the scaling problem and one more relation must be provided. Korst, in Reference 4, discusses four alternatives for this needed relation. The physical basis for these alternatives are: matching downstream wake recompression parameters from the Chapman-Korst flow model; matching momentum at corresponding plume boundaries; matching mass flux at corresponding plume boundaries; and matching plume boundary supersonic inviscid streamline deflection-pressure rise relations on the basis of local linearization. In Reference 5, Korst recommends use of this last principle which reduces to holding the parameter

$\frac{\gamma_p M_p^2}{M_p^2 - 1}$  constant between model and prototypes (this parameter is frequently

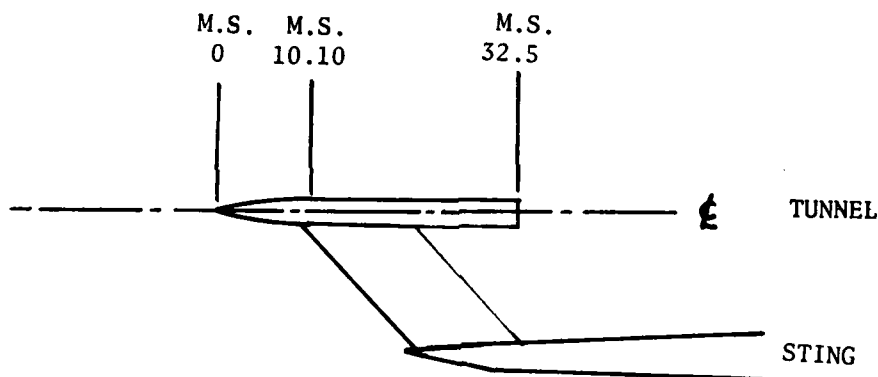
called the plume pliability parameter). In this parameter  $\gamma_p$  is the specific heat ratio for the jet and  $M_p$  is the Mach number along the plume boundary which is a constant when the jet issues into quiescent air. Implementation of the Korst scaling laws is greatly facilitated by use of a simplified theory, originally given by Johannesen & Meyer<sup>6</sup>, for calculation of the plume shape. This simplified theory is an integral part of the Korst scaling procedure in the sense that the inverse problem, arising in Korst's procedure, of determining the nozzle exit angle and Mach number to produce a given plume shape would be extremely difficult without this simplified theory.

The Korst modeling procedure has never been thoroughly correlated with experimental data. It was the original intent of the present program to provide the experimental data for such a correlation. In addition, the feasibility of modeling a jet plume by a solid afterbody extension, contoured to match the plume shape, was investigated. Four different nozzles which were designed to produce the same initial plume shape but with different values of the plume pliability parameter were tested and compared to the solid plume simulator. The Korst modeling procedure was to be verified by testing small scale rocket motors mounted in the base of the test model and comparing these results with tests on a model which was designed to be similar using air as the jet effluent. Both the small scale rocket motors and the air nozzles were to simulate the full scale operating conditions of the ZAP rocket motor. The tests on the small scale rocket motors were, however, deleted in anticipation of sled test data from full-scale ZAP firings. These data did not become available, which precluded a thorough evaluation of the Korst modeling laws in the present program; however, the data generated will provide a basis for comparison when full scale ZAP data becomes available. Moreover, the data acquired in the present program, along with some supplemental calculations using a more exact theory for plume shape allow an evaluation of the Johannesen-Meyer approximate plume theory. In addition, the comparison of the data on the plumes of different pliability parameters with the solid afterbody model data allows an assessment of this concept.

The wind tunnel tests were performed in the Calspan 8-Foot Transonic Wind Tunnel, and a detailed report on the wind tunnel tests, along with tabular data are presented in Reference 7. The intent of the present report is to present an analysis of the data. A brief description of the test will be given in Section II of this report for completeness. A comparison of the plume shapes calculated using Korst's approximate work to more exact calculations using the PIP Code<sup>8</sup> and to the experimental data will be presented in Section III. A comparison of afterbody pressure distribution with the solid plume simulator to those with the nozzles having varying plume pliability parameters will be presented in Section IV. Conclusions and recommendations will be presented in Section V.

## II. DESCRIPTION OF WIND TUNNEL TESTS

The wind tunnel tests are described in detail in Reference 7 and will be described only briefly here for the sake of completeness. The tests were conducted in the Calspan 8-Foot Transonic Wind Tunnel and consisted mainly of tests on six different rocket nozzles mounted in the aft end of a body of revolution. The body was mounted on a swept strut which was attached to a sting support system. The general arrangement is shown in the following sketch.



Air was supplied for the nozzles by plumbing in the sting and swept strut. The overall model length was 32.5 inches, of which 10.0 inches was an ogive nose and the remainder was a circular cylinder of 2.5 inches diameter. The nozzle nomenclature was designated by  $NC_y^x$  or  $NZ_y^x$  for the conical and simulated ZAP nozzles, respectively. The superscript,  $x$ , gives the ratio of nozzle exit diameter to body diameter and the subscript,  $y$ , gives the nominal exit Mach number. The nozzle coordinates are given in Tables 1 and 2.

The conical nozzles defined in Table 1 were all designed (by the Korst procedure) to produce the same plume shape when exhausting into quiescent air at their design pressure ratios. For purposes of these tests, the pertinent pressure ratio was defined as the ratio of jet total pressure to base pressure on the model. These design values were:

**Table 1**  
**CONICAL NOZZLE COORDINATES**

NC .8 1.7		NC .8 2.0		NC .8 2.4		NC .8 2.7	
d = 2.0000 d/D = 0.80 $\theta_i = 7.5^\circ$ $\theta_e = 9.10^\circ$		d = 2.0000 d/D = 0.80 $\theta_i = 15^\circ$ $\theta_e = 13.60^\circ$		d = 2.000 d/D = 0.80 $\theta_i = 15^\circ$ $\theta_e = 19.35^\circ$		d = 2.000 d/D = 0.80 $\theta_i = 15^\circ$ $\theta_e = 23.30^\circ$	
x	r	x	r	x	r	x	r
-.9560	.9600 <sup>①</sup>			-1.3681	.9600 <sup>①</sup>		
-.4889	.8985 <sup>②</sup>	-1.0061	.9600 <sup>①</sup>	-.4914	.7251 <sup>②</sup>		
-.4510	.8939	-.4944	.8229 <sup>②</sup>	-.4537	.7169		
-.4137	.8898	-.4535	.8159	-.4177	.7093		
-.3768	.8860	-.4133	.8096	-.3823	.7025		
-.3401	.8826	-.3736	.8039	-.3476	.6963	-1.5954	.9600 <sup>①</sup>
-.3035	.8795	-.3341	.7987	-.3129	.6907	-.5210	.6721 <sup>②</sup>
-.2666	.8767	-.2943	.7941	-.2785	.6857	-.4361	.6537
-.2299	.8743	-.2547	.7901	-.2435	.6812	-.3596	.6396
-.1922	.8722	-.2138	.7865	-.2089	.6773	-.2867	.6284
-.1282	.8695	-.1425	.7817	-.1724	.6738	-.2158	.6199
-.0641	.8679	-.0713	.7788	-.0862	.6681	-.1414	.6134
0	.8674 <sup>③</sup>	0	.7778 <sup>③</sup>	0	.6662 <sup>③</sup>	0	.6085 <sup>③</sup>
.0641	.8679	.0713	.7788	.0862	.6681	.1414	.6134
.1282	.8695	.1425	.7817	.1724	.6738	.2158	.6199
.1922	.8722	.2138	.7865	.2089	.6773	.2867	.6284
.2299	.8743	.2547	.7901	.2435	.6812	.3596	.6396
.2666	.8767	.2943	.7941	.2785	.6857	.4361	.6537
.3035	.8795	.3341	.7987	.3129	.6907	.5210	.6721
.3401	.8826	.3736	.8039	.3476	.6963	.6201	.6968
.3768	.8860	.4133	.8096	.3823	.7025	.7445	.7325
.4137	.8898	.4535	.8159	.4177	.7093	.9118	.7872
.4510	.8939	.4944	.8229	.4537	.7169	1.1533	.8771
.4889	.8985	.5615	.8355	.4914	.7251	1.4138	.9848 <sup>④</sup>
.5276	.9035	.6596	.8564	.5292	.7342	1.4491	1.0000 <sup>⑤</sup>
.5673	.9090	.7125	.8688 <sup>④</sup>	.5696	.7444		
.6084	.9152	1.2550	1.0000 <sup>⑤</sup>	.6121	.7558		
.6408	.9202 <sup>④</sup>			.6577	.7687		
1.1389	1.0000 <sup>⑤</sup>			.7071	.7835		
				.7608	.8004		
				.8194	.8199		
				.8620	.8346 <sup>④</sup>		
				1.3332	1.0000 <sup>⑤</sup>		

- ① NOZZLE ENTRANCE
- ② UPSTREAM TANGENT POINT
- ③ THROAT
- ④ DOWNSTREAM TANGENT POINT
- ⑤ NOZZLE EXIT

NOZZLE IS CONICAL BETWEEN ① AND ②, AND BETWEEN ④ AND ⑤, AT HALF ANGLES OF  $\theta_i$  AND  $\theta_e$ , RESPECTIVELY.

Nozzle	$P_t/P_b$
NC .8 1.7	39.6
NC .8 2.0	55.1
NC .8 2.4	82.4
NC .8 2.4	108.2

In addition to these nozzles, a solid plume simulator was tested, which was designed to simulate the plume produced by these nozzles.

The model ZAP nozzles were designed by the Korst procedure to simulate the plume for the full scale ZAP nozzle. The design pressure ratio for these models was 31.89.

The experimental measurements for all of the configurations tested consisted of afterbody pressure distributions over the rear 7.3 inches of the afterbody, base pressure measurements, jet total pressure, nozzle wall pressures, and schlieren photos of the plumes. The Mach number range encompassed by the tests was 0.4 to 1.25. The majority of these tests were run at zero degrees angle-of-attack, but a few runs were made at -5 degrees angle-of-attack.

Table 2  
MODEL ZAP NOZZLE COORDINATES

NZ .8 1.76		NZ .93 1.76	
$d = 2.0000$ $d/D = .80$ $\theta_i = 5^\circ$ $\theta_e = 3.95^\circ$		$d = 2.3168$ $d/D = .9267$ $\theta_i = 5^\circ$ $\theta_e = 3.95$	
x	r	x	r
-1.6018	.9600 <sup>①</sup>		
.4588	.8600 <sup>②</sup>		
.4088	.8575	-1.2483	1.1000 <sup>①</sup>
.3609	.8553	.4181	.9908 <sup>②</sup>
.3145	.8535	.3643	.9887
.2690	.8519	.3116	.9868
.2243	.8506	.2598	.9854
.1800	.8496	.2085	.9842
0	.8478 <sup>③</sup>	0	.9819 <sup>③</sup>
.1800	.8496	.2085	.9842
.2243	.8506	.2598	.9854
.2690	.8519	.3116	.9868
.3145	.8535	.3643	.9887
.3609	.8553	.4181	.9908
.4088	.8575	.4736	.9933
.4588	.8600	.5315	.9962
.5115	.8629	.5925	.9996
.5678	.8665	.6577	1.0037
.5998	.8686 <sup>④</sup>	.6948	1.0062 <sup>④</sup>
2.5022	1.0000 <sup>⑤</sup>	2.8986	1.1584 <sup>⑤</sup>

- ① NOZZLE ENTRANCE
- ② UPSTREAM TANGENT POINT
- ③ THROAT
- ④ DOWNSTREAM TANGENT POINT
- ⑤ NOZZLE EXIT

NOTE: INLET SECTION AHEAD OF NZ .93 NOZZLE IS EXPANDED TO 2.200 IN. DIA.  
1.76

### III. COMPARISON OF PLUME SHAPES

#### a) Discussion of the Calculation Procedure.

As mentioned in the introduction, the approximate plume theory of Johannesen & Meyer<sup>6</sup> is an important part of the Korst modeling procedure. This approximate theory has been evaluated by comparing the plume shapes calculated by it with more exact calculations and with schlieren photos taken during the wind tunnel tests.

There were primarily three areas of concern about the accuracy of the Johannesen-Meyer theory. The first area of concern was the mathematical assumptions explicitly made in the theory. The second area of concern was the starting line condition used in the nozzle throat area and the final area of concern was the neglect of the nozzle boundary layer. The Johannesen-Meyer theory is an approximate solution to the equations of motion for isentropic flow based upon a coordinate expansion scheme employing the radial distance centered at the nozzle exit lip as a small quantity. On this basis, one would expect that the approximations involved would break down at distances farther than one exit radius from the nozzle exit.

In any of the nozzle flow calculation procedures, velocity data is needed on a start line which is located just downstream of the nozzle throat in the fully supersonic portion of the flow. There are several methods available for generating this initial data as discussed in Reference 9. The simplest method, and the method used by Korst, is to assume that the flow down stream of the nozzle throat is source-like producing flow tangent to the nozzle wall at a prescribed point.

These first two areas of concern have been investigated by comparing the plume shapes calculated by the Korst procedure with calculations made by the P.I.P.<sup>8</sup> code which employs the method of characteristics. The method of characteristics represents an "exact" numerical solution to the equations of motion. Various start line conditions were used with the P.I.P. code to evaluate this effect.

For high Reynolds number flows, the nozzle wall boundary layer will have only a small influence upon the flow within the nozzle, but may have a significant effect upon the initial divergence angle of the plume. The boundary layer produces a low Mach number region next to the wall, and as a result the angle of the Prandtl-Meyer expansion required at the nozzle lip to attain the free stream static pressure is larger than in the inviscid case. As previously noted, the Johannesen-Meyer theory does not account for the nozzle boundary layer. The P.I.P. code contains, as an option, an empirical method of estimating the nozzle boundary layer thickness and velocity profile. This method is based upon the correlation of boundary layer thickness parameters that was developed in Reference 10. Calculations made with and without the boundary layer present then gives an evaluation of boundary layer effects. The method of calculation used by the P.I.P. code is discussed in the following.

All calculations were started from an input initial line just downstream of the throat and were continued to the nozzle exit using the Hartree form of the method-of-characteristics. Since this procedure uses a mesh composed of streamlines and normals instead of the well known characteristics net, imbedded shocks, which are ordinarily detected by the crossing of characteristics of the same family, do not create numerical problems and appear in the flow field as isentropic compressions.

At the nozzle exit, the calculation may be interrupted in order to introduce the effects of a nozzle boundary layer. The procedure for simulating this boundary layer involves identifying a point on the assumed velocity-temperature profile having a prescribed supersonic Mach number  $M_0$  and applying a stretching transform which moves the  $M_0$  point to the nozzle lip. In this process, the fluid for which  $M < M_0$  is essentially removed from the flow so it is desirable to make  $M_0$  as small as possible. On the other hand, experience has shown that numerical difficulties appear in the subsequent exterior flow calculation if  $M_0$  is too small. Therefore, a compromise value of  $M_0 = 1.20$  was adopted for all cases reported here.

After restarting the plume calculation from the modified initial line, a Prandtl-Meyer expansion is calculated terminating at the ambient pressure. As this expansion is performed in several stages, a multiple point is created at the nozzle lip. From each of these coincident points, a right-running characteristic is intersected with a line normal to the flow direction at the previous point. A new streamline is started from each of these intersections. In this way, a grid of streamlines and normals is built up.

From each interior point of this grid, characteristics are drawn backward to intersect the previous normal line. Linear interpolation provides the flow conditions at each of these base points and simultaneous solution of the compatibility equations along these characteristics and along the streamline provides the flow conditions at the new grid point.

Only one characteristic is needed to calculate the boundary points. On the axis, of course, the flow direction is prescribed and at the outer boundary, the plume pressure must match the ambient exterior pressure.

Several series expansion methods for generating the required nozzle starting line data are reviewed and extended in Reference 9. The three series expansion methods are basically due to Sauer<sup>11</sup>, Hall<sup>12</sup>, and Kliegel and Levine<sup>13</sup>. In the present program, calculations of the starting line data were made using all three of these methods at a station downstream of the nozzle throat where the area ratio was 1.025. The Hall method resulted in the best satisfaction of flow tangency at the nozzle wall and was consequently used for most of the computations. In addition, a source line start was used for a few cases in order to evaluate the two starting line procedures.

### b) Results of Calculations

The calculations discussed above were made for the four nozzles described in Table I, operating at their design pressure ratios. The results are presented in Figures 1 through 6 wherein the Korst plume shape is compared to various calculations made using the P.I.P. code. For Figures 1 through 4, the P.I.P. code calculations, were started from the Hall starting line values and the calculations were made with and without accounting for the nozzle boundary layer. The agreement between the approximate plume shape and the P.I.P. code calculations that ignore the nozzle boundary layer is quite good for the first several exit radii downstream of the exit. The agreement this far downstream of the exit is surprising, considering the mathematical approximations used in the Johannesen-Meyer theory. As expected, the P.I.P. code calculations show that the effect of the nozzle boundary layer is to fatten the plume shapes. This effect is significant for the two highest exit Mach number nozzles (Figures 3 and 4). The approximate plume shape is generally slightly fatter than the P.I.P. code results without a boundary layer. The inclusion of the boundary layer compensates for this slight difference for the lower exit Mach number nozzles.

The effect of nozzle starting line values has been investigated by running the P.I.P. code with various starting line conditions. The results for the lowest exit Mach number nozzle and the highest exit Mach number nozzle are shown in Figures 5 and 6, respectively. It may be seen that all of the starting line conditions used, resulted in essentially the same plume shape. Thus, it may be concluded that the simpler source flow starting conditions are adequate for calculating the nozzle and plume flows.

### c) Comparison With Schlieren Photos

The calculated plume shapes would not be expected to agree precisely with the experimental observations because the calculations ignore the interaction between the plume and the surrounding flow. However, comparison of the calculated plume shapes to the schlieren photos shows that the calculated shapes are an amazingly good approximation to the resultant plume shapes. Schlieren photos for the four nozzles defined in Table I, are shown in Figures 7 through 10. Only the highest and lowest free stream Mach numbers tested for each nozzle have been selected for presentation as the remaining photos show similar results. In each of the figures presented, the Korst plume shape has been overlaid on the photos. The general features of the plume flow appear to be consistent with previous observations on similar under-expanded plumes. (See, for example, the sketches and photos presented in References 14 and 15.) The sharp lines that lie inside the Korst plume shape are the barrel shocks. The barrel shock usually terminates in the so-called Mach disk or nearly normal shock. The Mach disk is visible in Figure 7a, but occurs out of the field-of-view in the other figures. The outer edge of the plume is not visible as a sharp line as, undoubtedly, the viscous mixing between the jet and surrounding flow has weakened the density gradient in the flow. Even though the outer plume boundary is not clearly definable in most of

the photos, it is evident that the Korst plume shape is a reasonable approximation to the actual plume shape for the portion of the plume in view. Evidently, for these conditions, the interaction of the plume with the surrounding flow produces little alteration in the plume shape. The agreement of the calculated plume shape in which the interaction with the surrounding flow is neglected, with the actual plume shape suggest that both the inviscid interaction and viscous mixing between the plume and free stream are not important for the initial region of plume development. Moreover, the agreement also suggests that a theoretical treatment accounting for the inviscid interaction could be based upon a linearized correction to the non-interacting plume solution.

In some of the schlieren photos, a slight upward tilting of the barrel shock pattern, on the order of a degree, may be noted. This suggests that the swept strut on the bottom of the model may have a slight influence on the plume shape. Examination of the photos shows another abnormality. A dark tongue may be observed extending from the lower lip of the nozzle exit on all the schlieren photos. Its appearance varies from the extremely obvious such as in Figure 10a to barely noticeable as in Figures 7a and 7b. It is presently not known whether this tongue is an anomaly of the schlieren system or an actual flow disturbance. There is no large scale disturbance of the plume associated with it, and since the pressures on the afterbody are taken on top of the model, they are believed to be unaffected.

#### d) Nozzle Pressure Distributions

There were four pressure taps located within the nozzle on its upper surface. The measurements made with these taps have been compared with calculations from the P.I.P. code as a check on the validity of the data. The results are presented in Figures 11 through 14. The solid line in each of these figures was calculated from the P.I.P. code using the Hall starting line. As can be seen, the experimental pressures correlate quite well with calculations which suggests that there are no abnormalities in the nozzle flow. Only the data corresponding to the design condition has been shown. The nozzle pressure measurements from many of the runs were checked and for all practical purposes, these data fall on top of the data presented.

#### IV. AFTERBODY PRESSURE DISTRIBUTIONS

##### a) Similar Plume Shape Models

The afterbody pressure distribution associated with those nozzles that were designed to give the same plume shape are presented in Figures 15 through 20 at zero degrees angle-of-attack. The solid plume simulator is designated by  $S_2$  and shown for those cases for which the data are available. There were ten pressure taps on the cylindrical afterbody of the model, beginning at 7.312 inches ahead of the body base. The location of the foremost tap has been selected as the origin for  $X$ . The aftmost point shown in these figures is a base pressure measurement. The base pressure tap was located at a radial station of 1.095 inches from the model center line. The tap was located approximately halfway between the nozzle lip and the body shoulder.

Since the nozzles were all designed to produce the same plume shape when they were discharging into quiescent air, these figures show the influence of the plume pliability parameter on the afterbody pressures. The parameter defined as

$K = \frac{\gamma M_p^2}{M_p^2 - 1}$  is given for the various nozzles below.

Nozzle	K	$M_p$
NC <sup>.8</sup> <sub>1.7</sub>	4.5693	3.088
NC <sup>.8</sup> <sub>2.0</sub>	4.7991	3.263
NC <sup>.8</sup> <sub>2.4</sub>	5.1904	3.558
NC <sup>.8</sup> <sub>2.7</sub>	5.4526	3.754

This parameter is essentially  $\frac{1}{\rho} \frac{dP}{d\theta}$  along the plume boundary where  $P$  is the static pressure and  $\theta$  is the angle of the tangent to the plume boundary. The data show that increasing this parameter systematically increases the pressure on the afterbody as far forward on the model as the measurements were made. The influence of this parameter is most pronounced in the supersonic results (Figures 19 and 20). The data suggests that there is a shock present on the afterbody (confirmed by schlieren photos) and the shock position is influenced by the plume pliability parameter.

Generally at zero degrees angle of attack, with the exception of  $M_\infty = 0.4$ , it is seen that the solid plume simulator gives a good simulation of the plume effects on the afterbody for the higher values of the plume pliability parameter. Unfortunately the degree of simulation deteriorates with angle of attack as demonstrated by Figure 21 wherein it is seen that the pressures near the shoulder of the body diverges for the two simulations.

The pressure distributions for all of these design cases do not show any plateaus which would be indicative of separation on the model afterbody. For the most part the flow adjacent to the body is monotonically decelerated as the body shoulder is approached and the base pressures are all above ambient static. It seems then that any conclusions about the validity of representing a plume with a solid body should be tempered to exclude, at least presently, cases where afterbody separation is present. Nevertheless the solid plume simulator seems to give good results for zero angle of attack when the plume pliability parameter is high enough (say  $K > 5$ ).

The data taken on the nozzles at all pressure ratios was surveyed to ascertain if separation had occurred on the afterbody under any of the circumstances tested. In general it appeared that separation was not encountered for any of the nozzles except on the highest pressure ratios tested at  $M_p = 1.25$ . Typical results for the off-design pressure ratios at subsonic free stream speeds are shown in Figures 22 and 23. It is seen that increasing the jet total pressure systematically increases the afterbody pressures. A typical result for supersonic speeds is shown in Figure 24. Here it is seen that increasing the jet total pressure systematically pushes the shock forward and finally for the highest pressure ratio tested the plateau in the pressure distribution near the body shoulder suggests a separation.

#### b) Validation of the Korst Modeling Procedures

The experimental validation of the Korst modeling procedure would require testing of different nozzles designed to give the same plume shape and same value of the plume pliability parameter. It would appear that choosing different gases for the jet effluent and thereby varying  $\gamma$  between the two tests would be the best way to accomplish this. However, it is theoretically possible to use a common effluent and still make the comparison. This possibility arises because for fixed  $\gamma$  and  $K \neq 2.0$ , two different plume boundary Mach numbers give the same value of  $K$ . This is illustrated by the following table calculated for the cases tested in the present program.

Nozzle	K	$M_p$	M-
NC <sup>8</sup> <sub>1.7</sub>	4.5693	3.088	1.0569
NC <sup>8</sup> <sub>2.0</sub>	4.7991	3.263	1.0506
NC <sup>8</sup> <sub>2.9</sub>	5.1904	3.558	1.0420
NC <sup>8</sup> <sub>2.7</sub>	5.4526	3.754	1.0375

Here  $M_p$  is the design plume Mach number (tested) and M- is the other Mach number<sup>p</sup> (not tested) that would produce the same value of  $K$ . However, inspection of the range of values of M- shows that any nozzles designed using this method of validating Korst's modeling procedure would have to be designed with

extreme accuracy. Furthermore since these values of  $M_{-}$  are so close to sonic the tendency toward normal shock formation in the plume could easily invalidate the comparison.

c) ZAP Models

Finally the afterbody pressure distribution on the ZAP models is presented in Figures 25 and 26 in order to facilitate correlations when the full scale ZAP data becomes available.

## V. CONCLUSIONS AND RECOMMENDATIONS

An experimental program to evaluate the effects of various plume parameters, for underexpanded jets, on missile afterbody pressure distributions has been conducted. Analysis of the experimental results and supplemental calculations made by the method of characteristics show that the approximate theory used by Korst gives a good estimate of the plume shape for nozzle exit Mach numbers of 2.0 and below. For nozzle exit Mach numbers much in excess of 2.0 it appears desirable to include the effect of the nozzle wall boundary layer on plume shape.

In addition, afterbody pressure distributions produced by a series of nozzles designed to produce the same plume shape, but with different values of the plume pliability parameter, have been compared with results from a solid plume simulator. In general, the solid plume simulator produces results that agree with the nozzles with the higher values of the plume pliability parameter at zero degrees angle-of-attack. The correlation deteriorates significantly, however, at five degrees angle-of-attack.

Finally, afterbody pressure distribution from model tests on the ZAP rocket motor are presented for future correlation with prototype results.

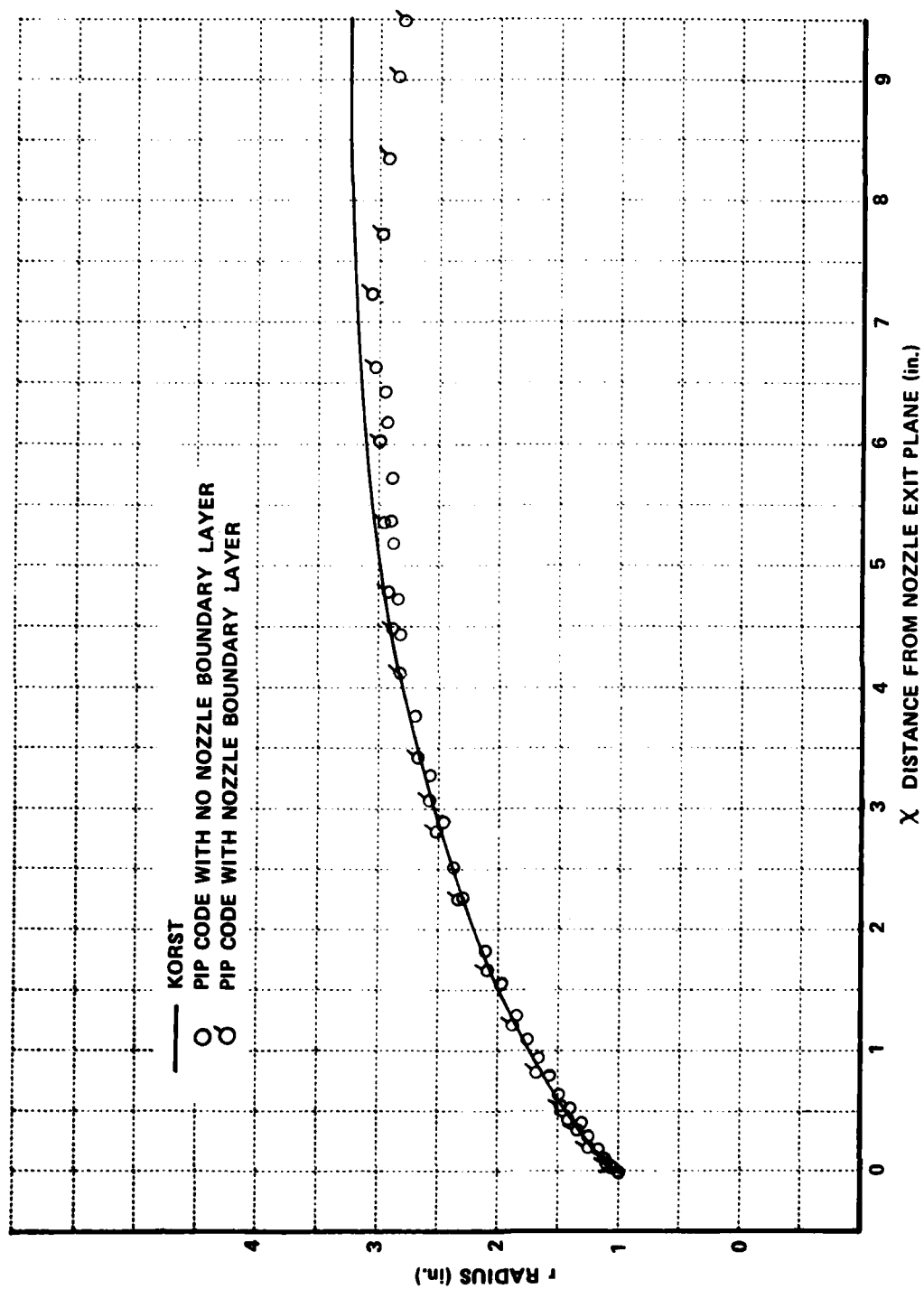


Figure 1 COMPARISON OF CALCULATED PLUME SHAPES, NOZZLE NC.8<sub>1.7</sub>

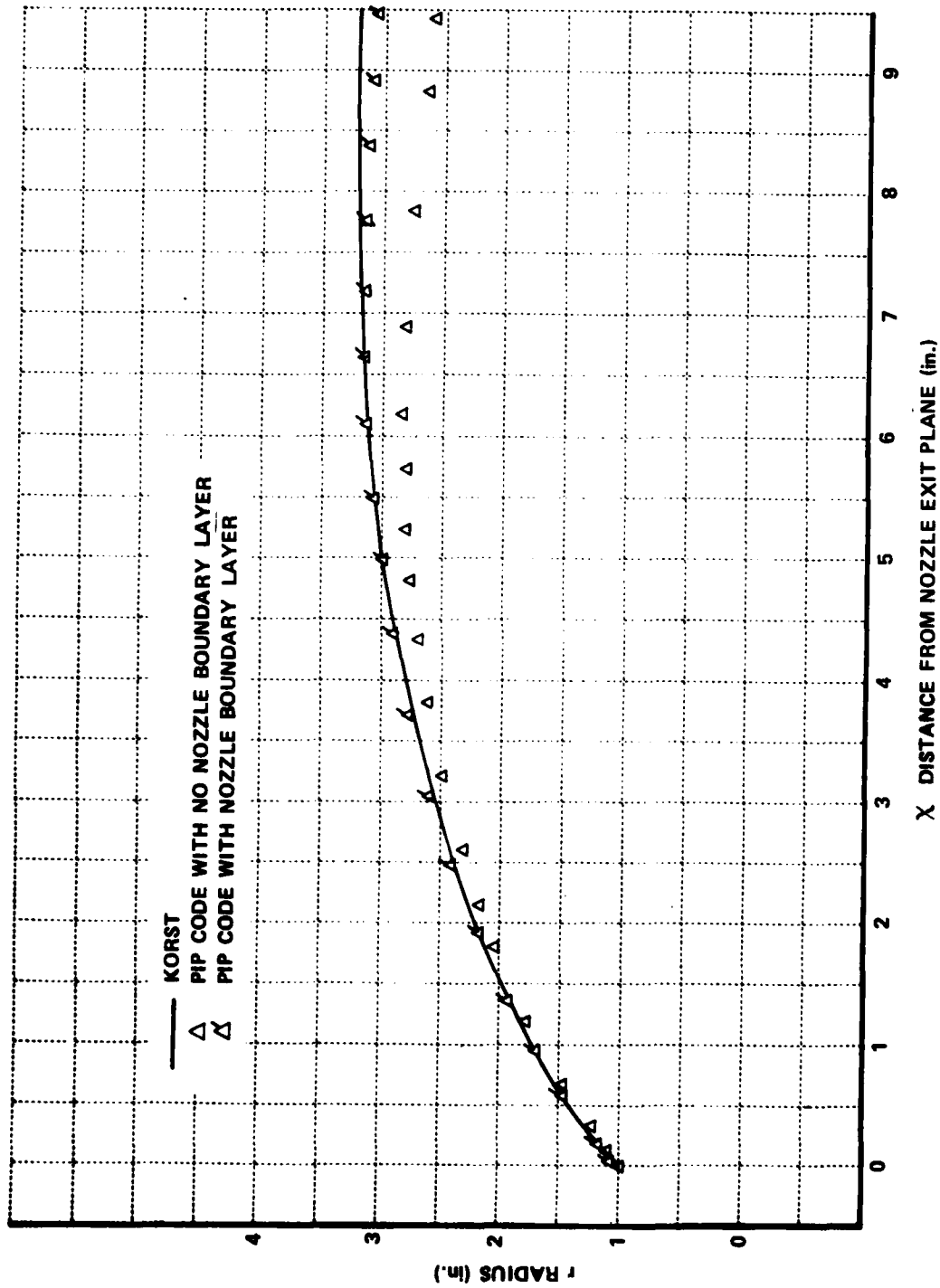


Figure 2 COMPARISON OF CALCULATED PLUME SHAPES, NOZZLE NC.8<sub>2.0</sub>

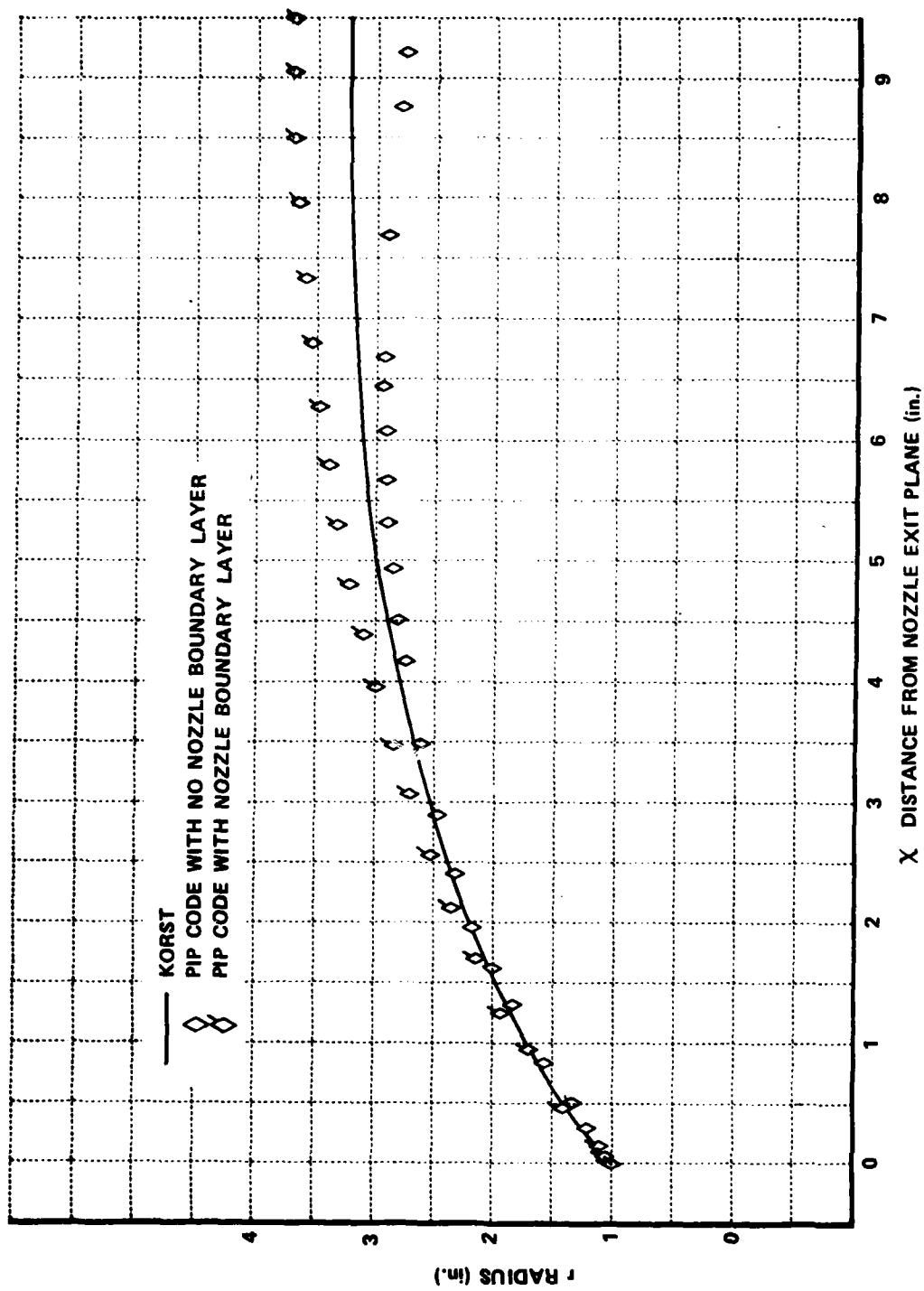


Figure 3 COMPARISON OF CALCULATED PLUME SHAPES, NOZZLE NC.8<sub>2.4</sub>

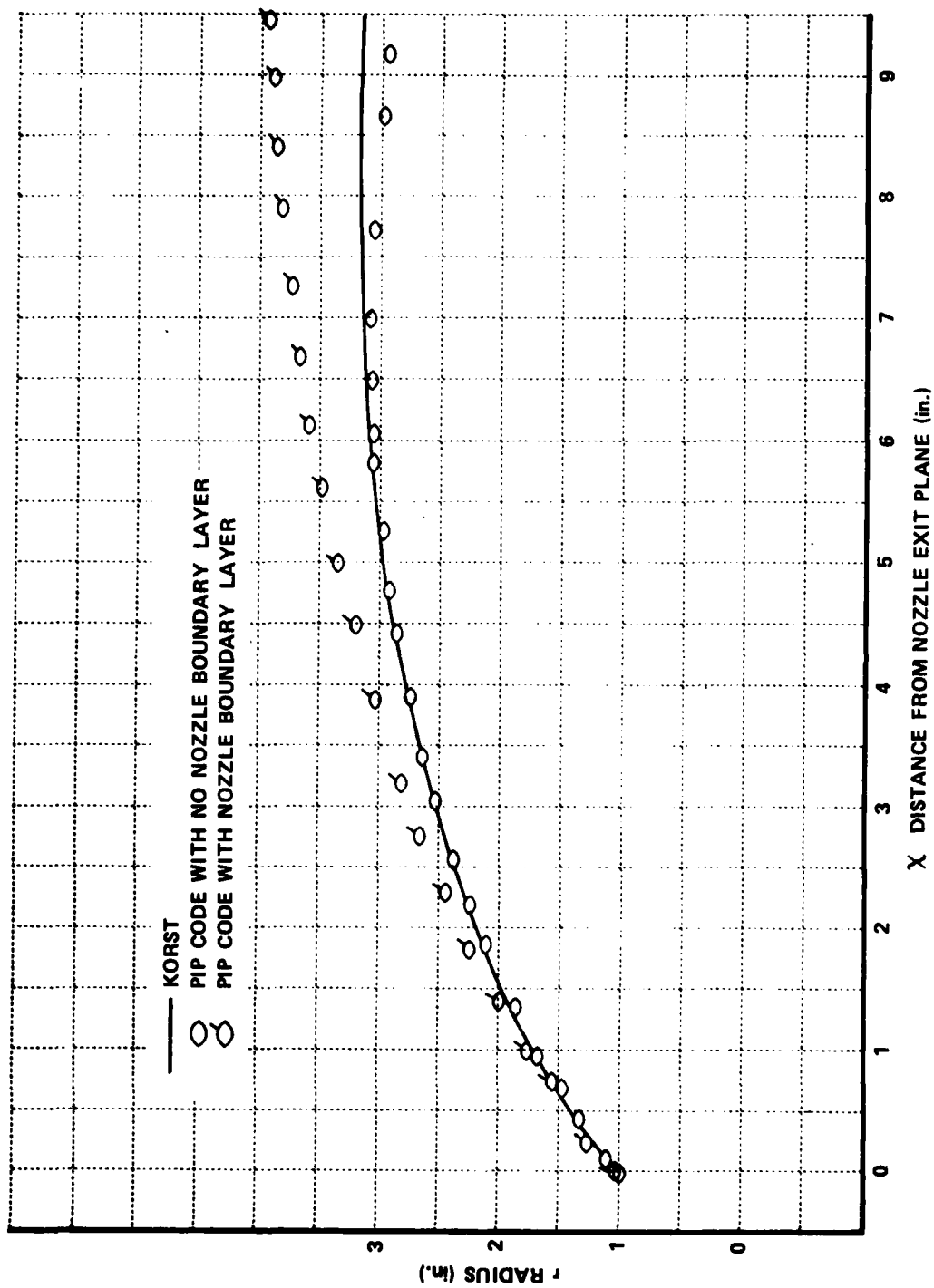


Figure 4. COMPARISON OF CALCULATED PLUME SHAPES, NOZZLE NC<sub>2.7</sub><sup>8</sup>

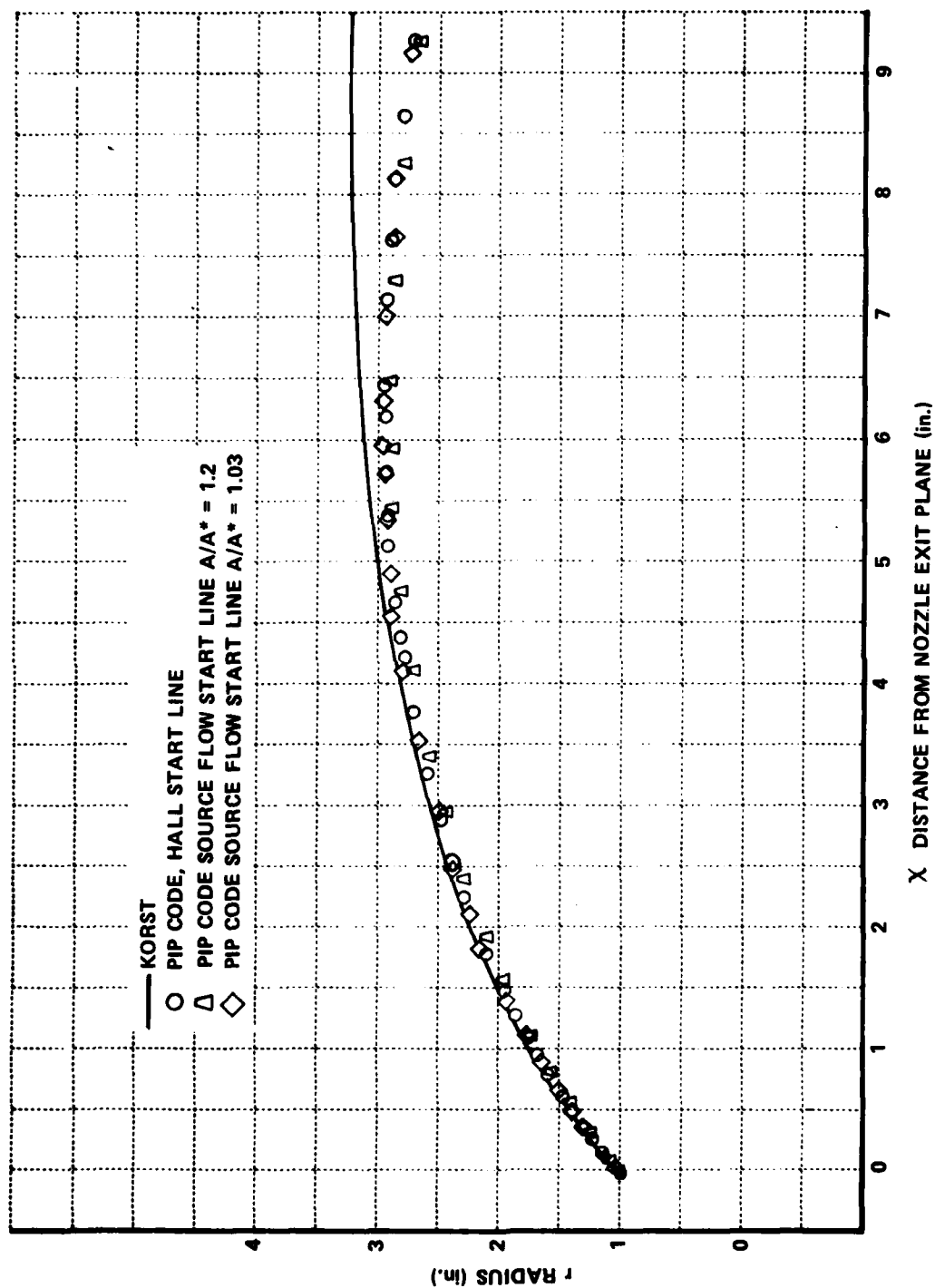


Figure 5 EFFECT OF NOZZLE STARTING LINE CONDITIONS ON PLUME SHAPE,  
NOZZLE NC<sub>1.7</sub> WITH NO NOZZLE BOUNDARY LAYER

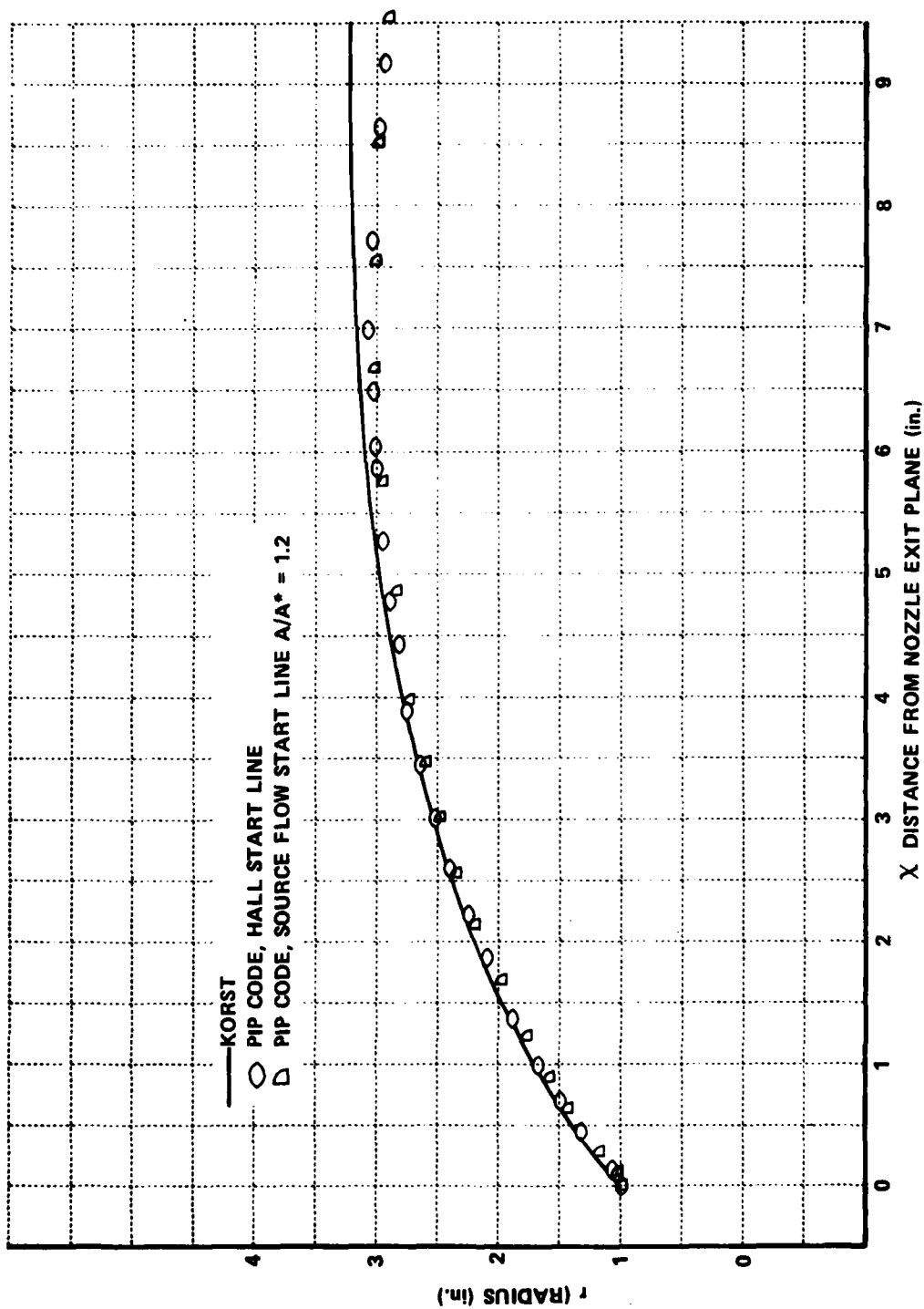
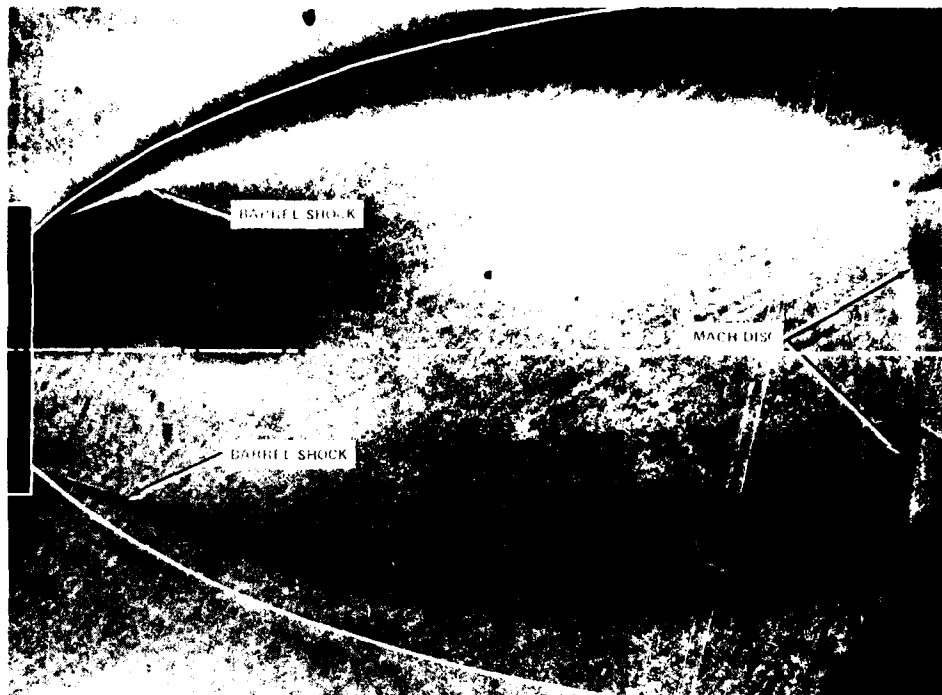


Figure 6 EFFECT OF NOZZLE STARTING LINE CONDITIONS ON PLUME SHAPE,  
NOZZLE NC<sub>2.7</sub> WITH NO NOZZLE BOUNDARY LAYER



a)  $M_{\infty} = 0.4$



b)  $M_{\infty} = 1.25$

Figure 7 COMPARISON OF KORST PLUME SHAPE WITH EXPERIMENT,  
NOZZLE NC<sub>1.7</sub><sup>8</sup>,  $P_c/P_b = 39.6$



a)  $M_{\infty} = 0.4$



b)  $M_{\infty} = 1.25$

Figure 8 COMPARISON OF KORST PLUME SHAPE WITH EXPERIMENT,  
NOZZLE NC-8  
2.0,  $P_c/P_b = 55.1$



a)  $M_\infty = 0.4$



b)  $M_\infty = 1.25$

Figure 9 COMPARISON OF KORST PLUME SHAPE WITH EXPERIMENT,  
NOZZLE NC-8  
2.4',  $P_c/P_b = 82.4$



a)  $M_{\infty} = 0.4$



b)  $M_{\infty} = 1.25$

Figure 10 COMPARISON OF KORST PLUME SHAPE WITH EXPERIMENT,  
NOZZLE NC.8  
2.7,  $P_c/P_b = 108.2$

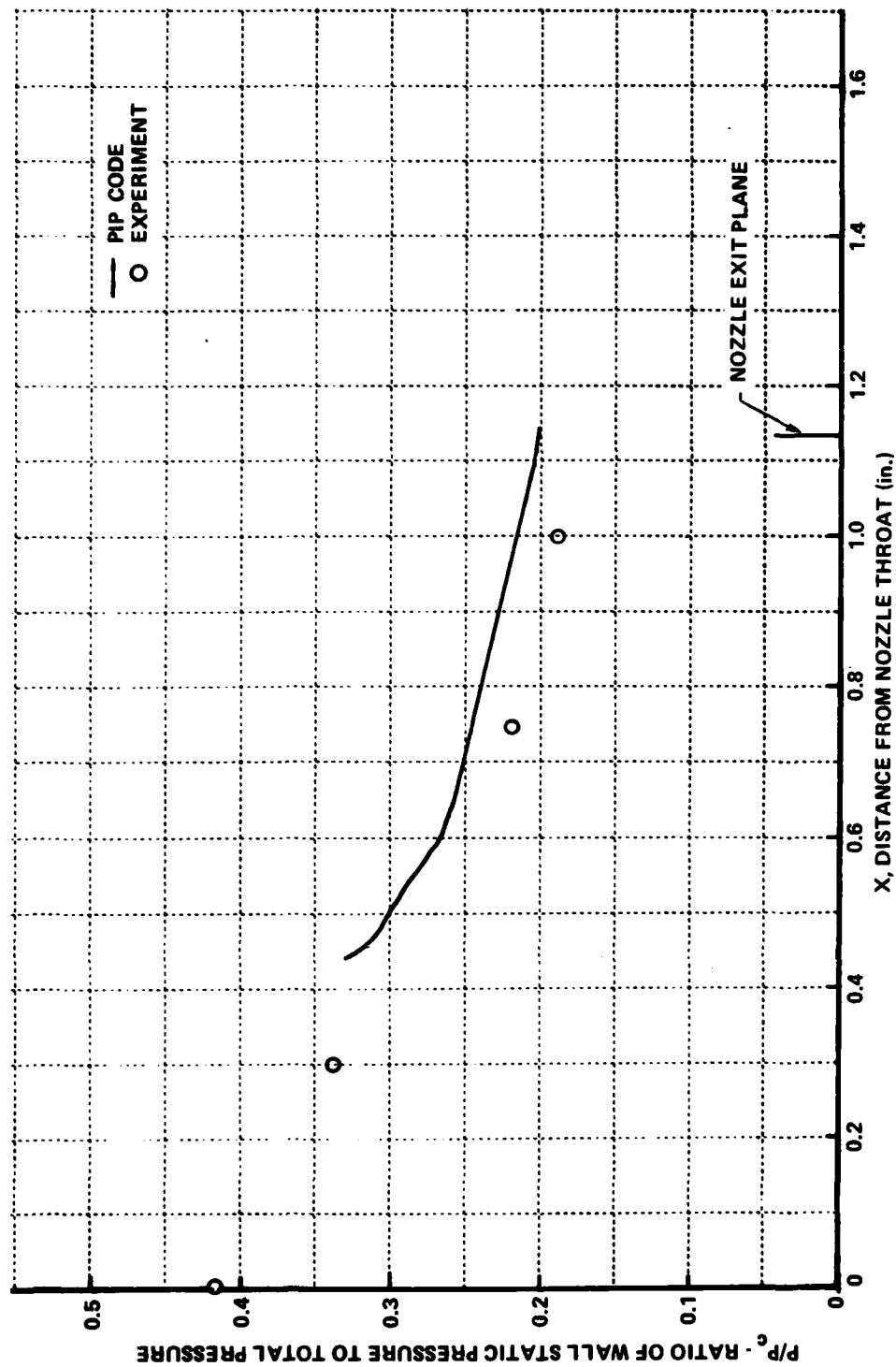


Figure 11 NOZZLE WALL PRESSURE DISTRIBUTION - NOZZLE NC 1.7

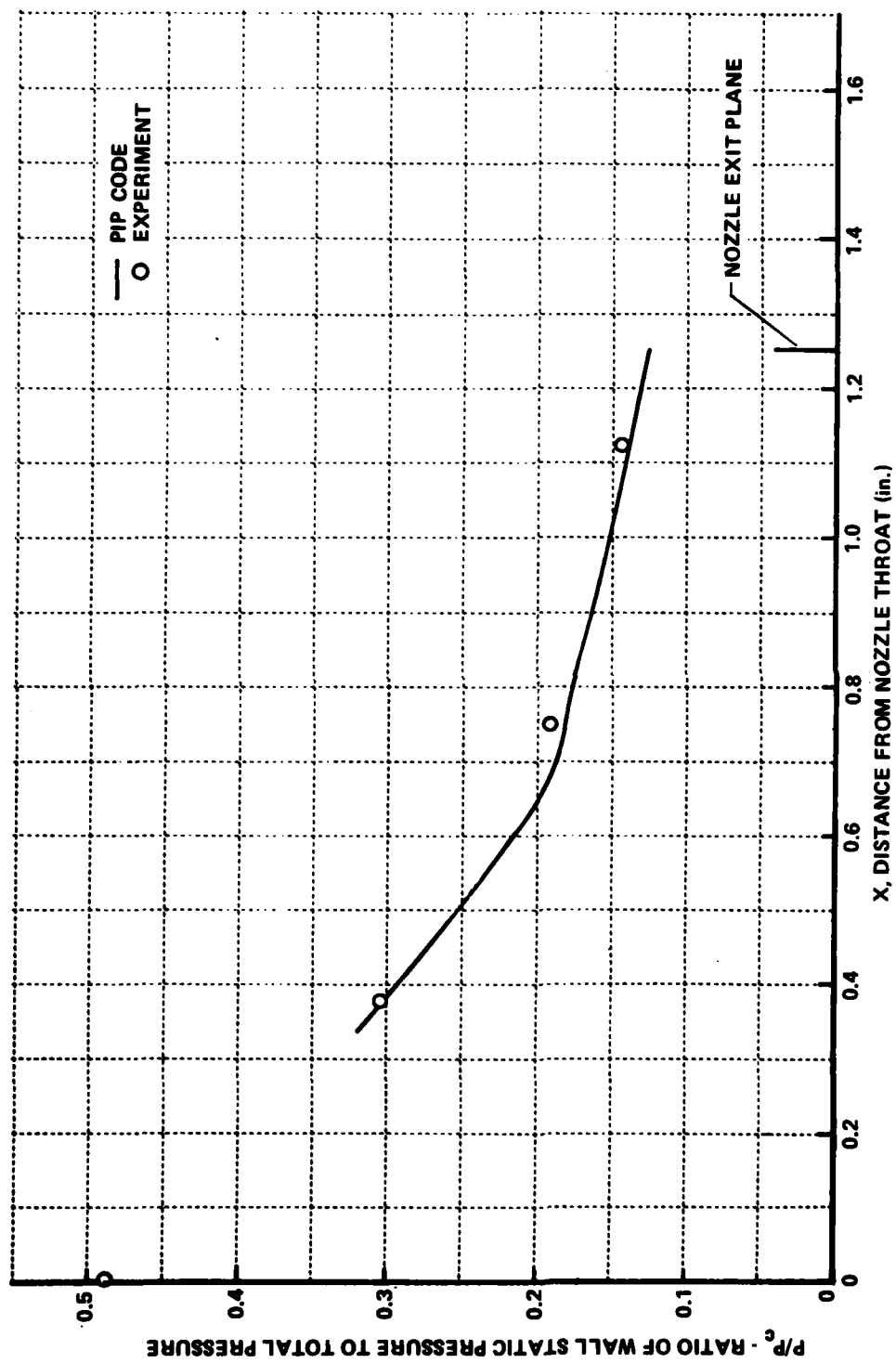


Figure 12 NOZZLE WALL PRESSURE DISTRIBUTION - NOZZLE NC .8  
2.0

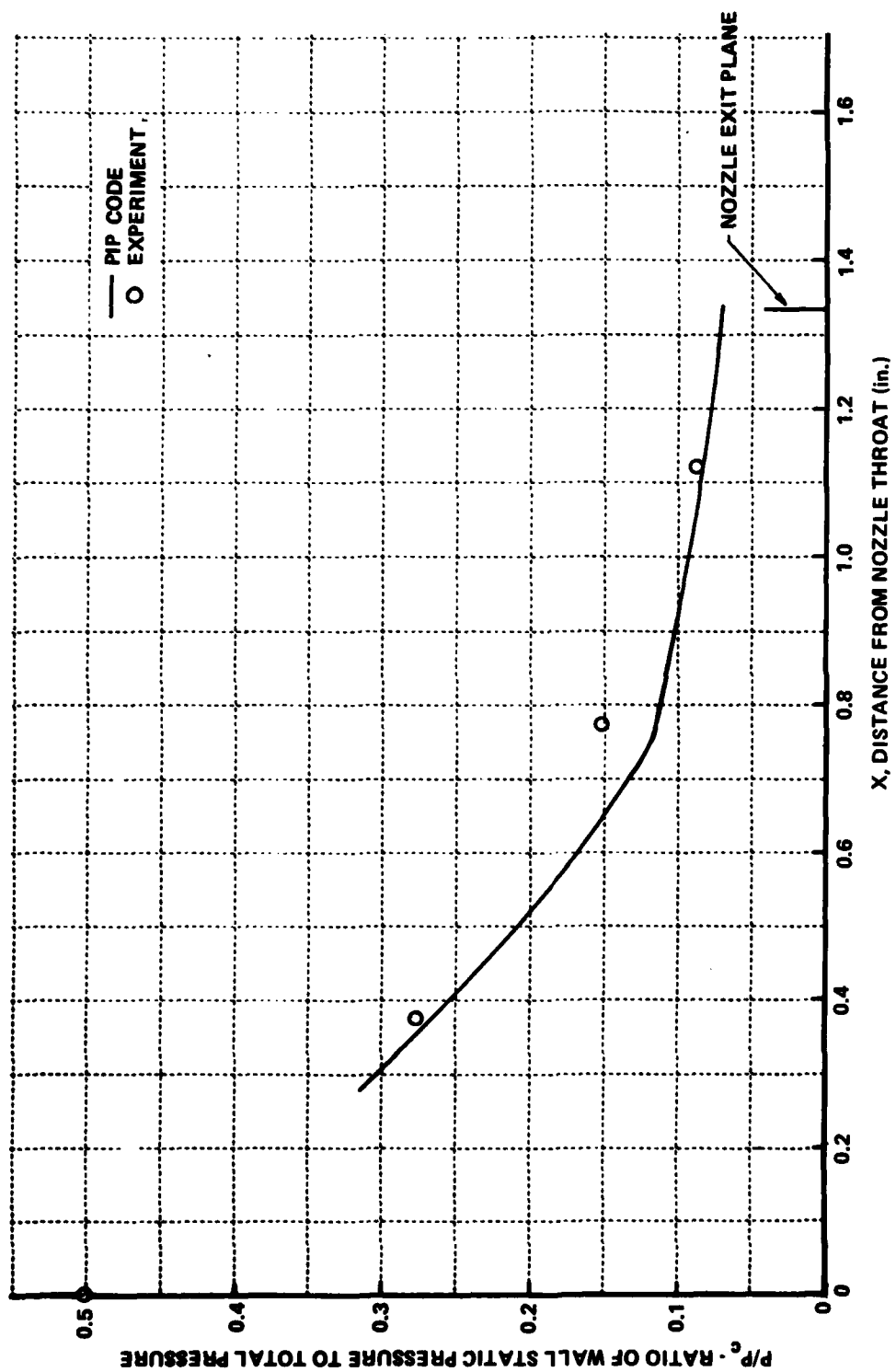


Figure 13 NOZZLE WALL PRESSURE DISTRIBUTION - NOZZLE NC .8  
2.4

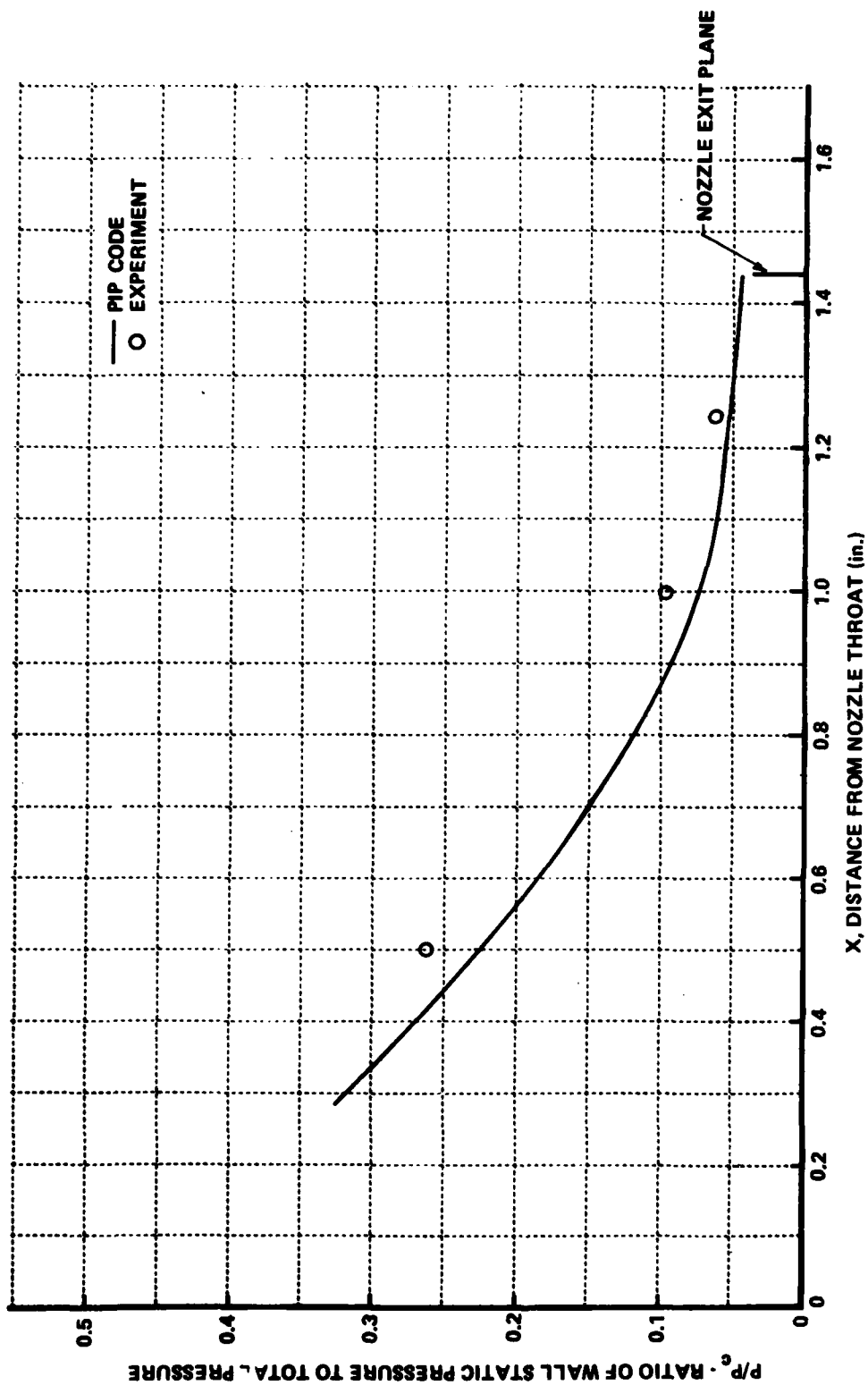


Figure 14 NOZZLE WALL PRESSURE DISTRIBUTION - NOZZLE NC 2.7 .8

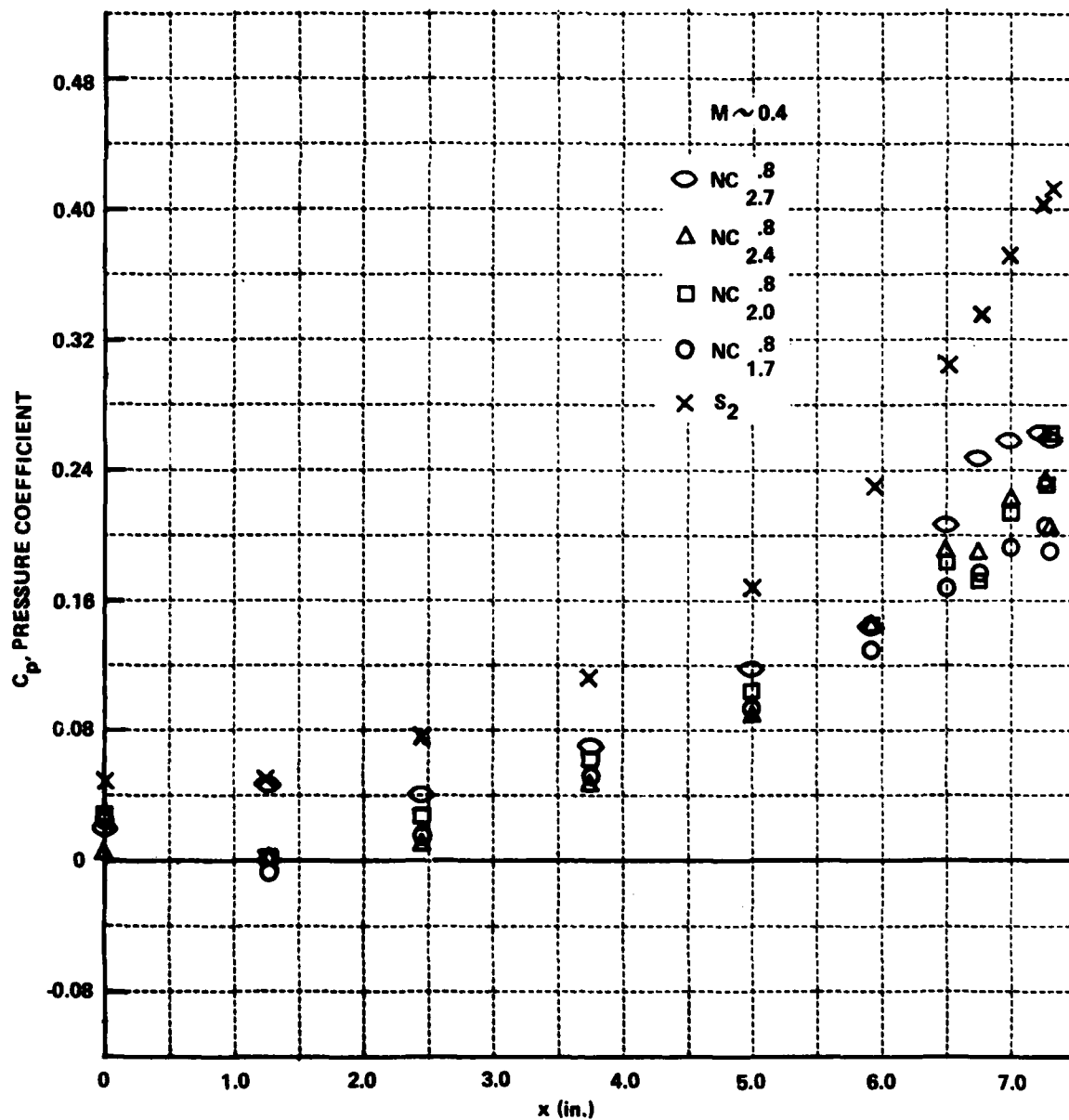


Figure 15 COMPARISON OF AFTERBODY PRESSURE DISTRIBUTIONS WITH ROCKET NOZZLES OPERATING AT DESIGN VALUES -  $M_\infty = 0.4$

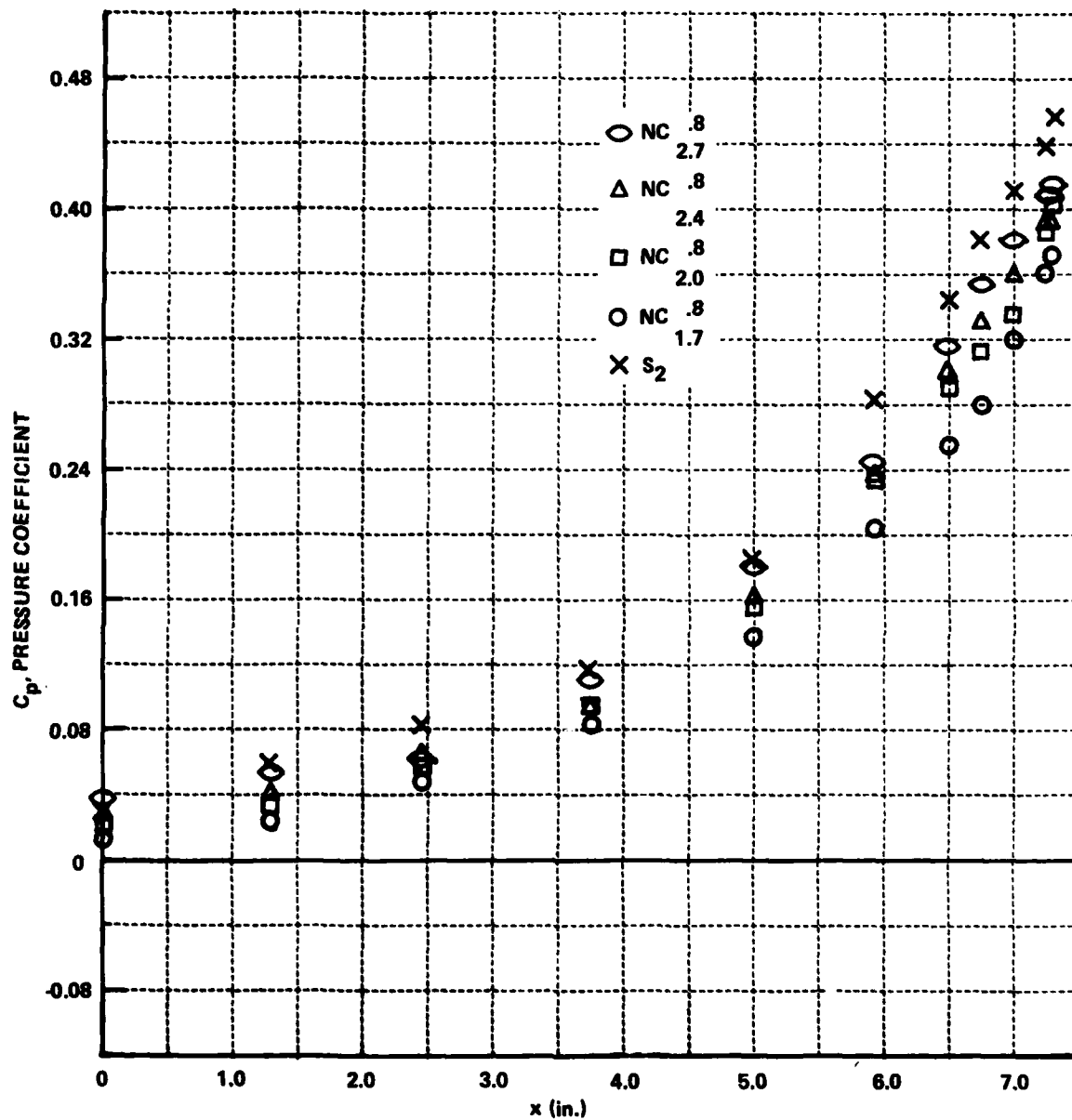


Figure 16 COMPARISON OF AFTERBODY PRESSURE DISTRIBUTIONS WITH ROCKET NOZZLES OPERATING AT DESIGN VALUES -  $M_\infty = 0.7$

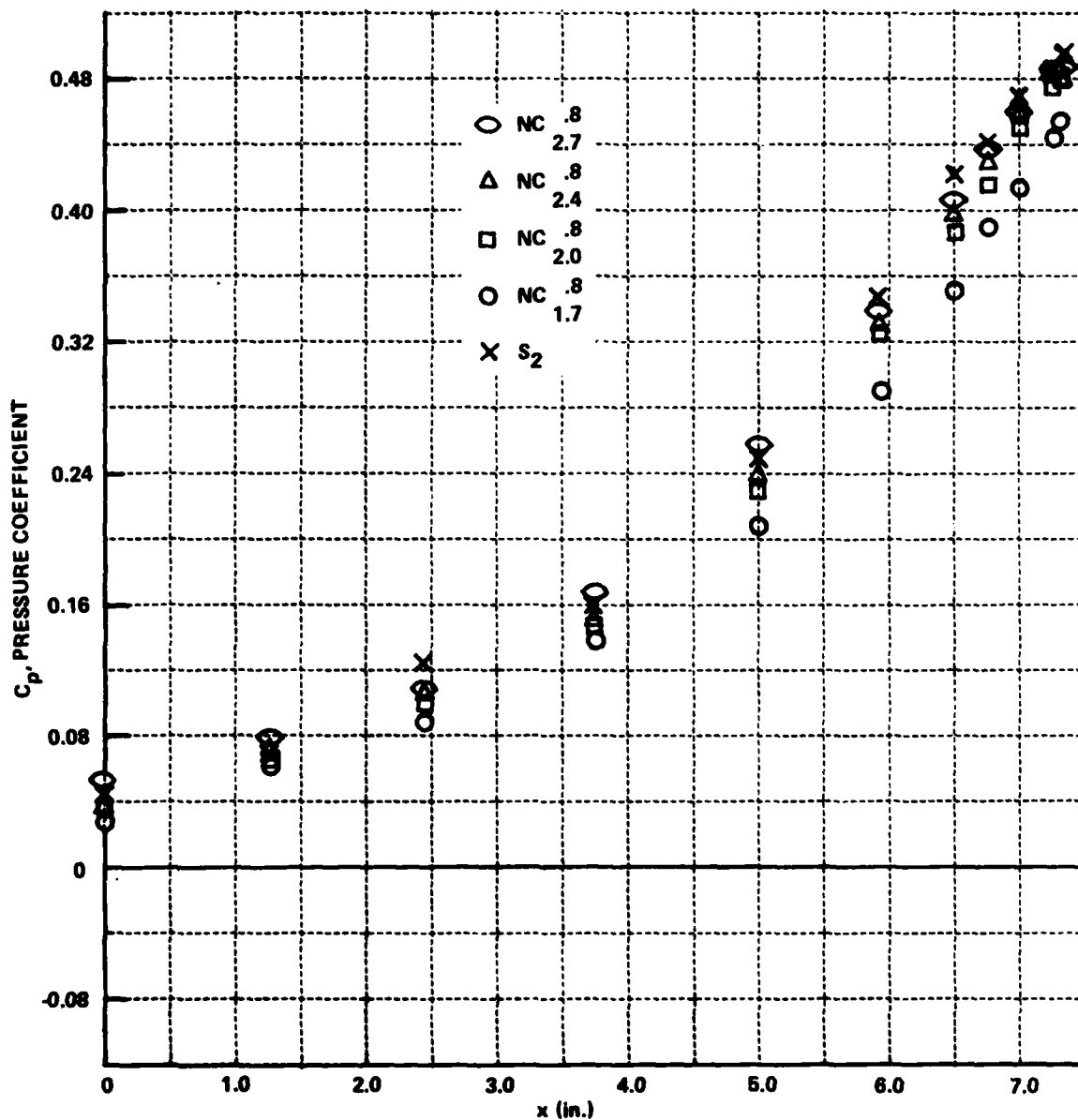


Figure 17 COMPARISON OF AFTERBODY PRESSURE DISTRIBUTIONS WITH ROCKET NOZZLES OPERATING AT DESIGN VALUES -  $M_{\infty} = 0.9$

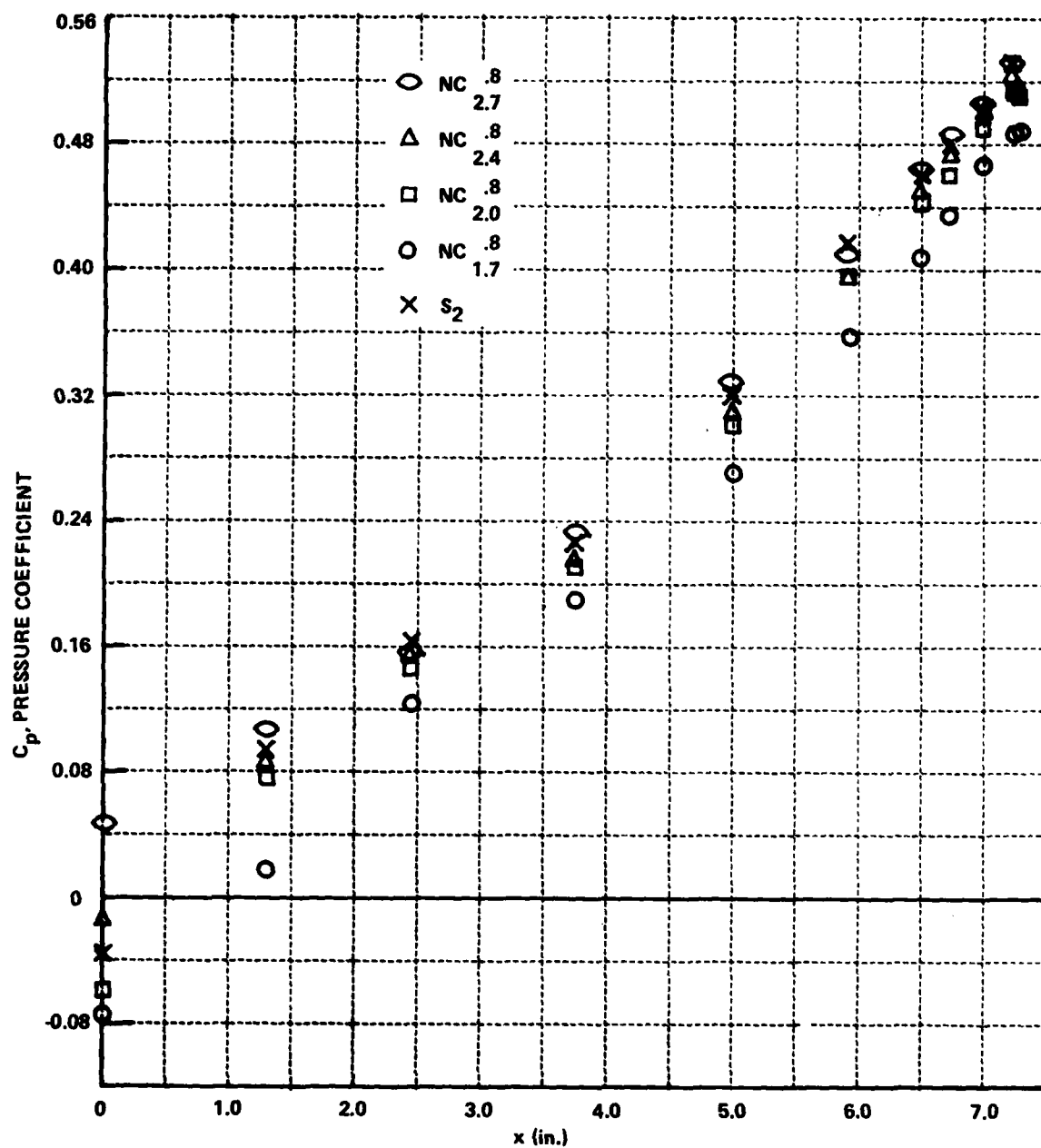


Figure 18 COMPARISON OF AFTERBODY PRESSURE DISTRIBUTIONS WITH ROCKET NOZZLES OPERATING AT DESIGN VALUES -  $M_{\infty} = 1.001$

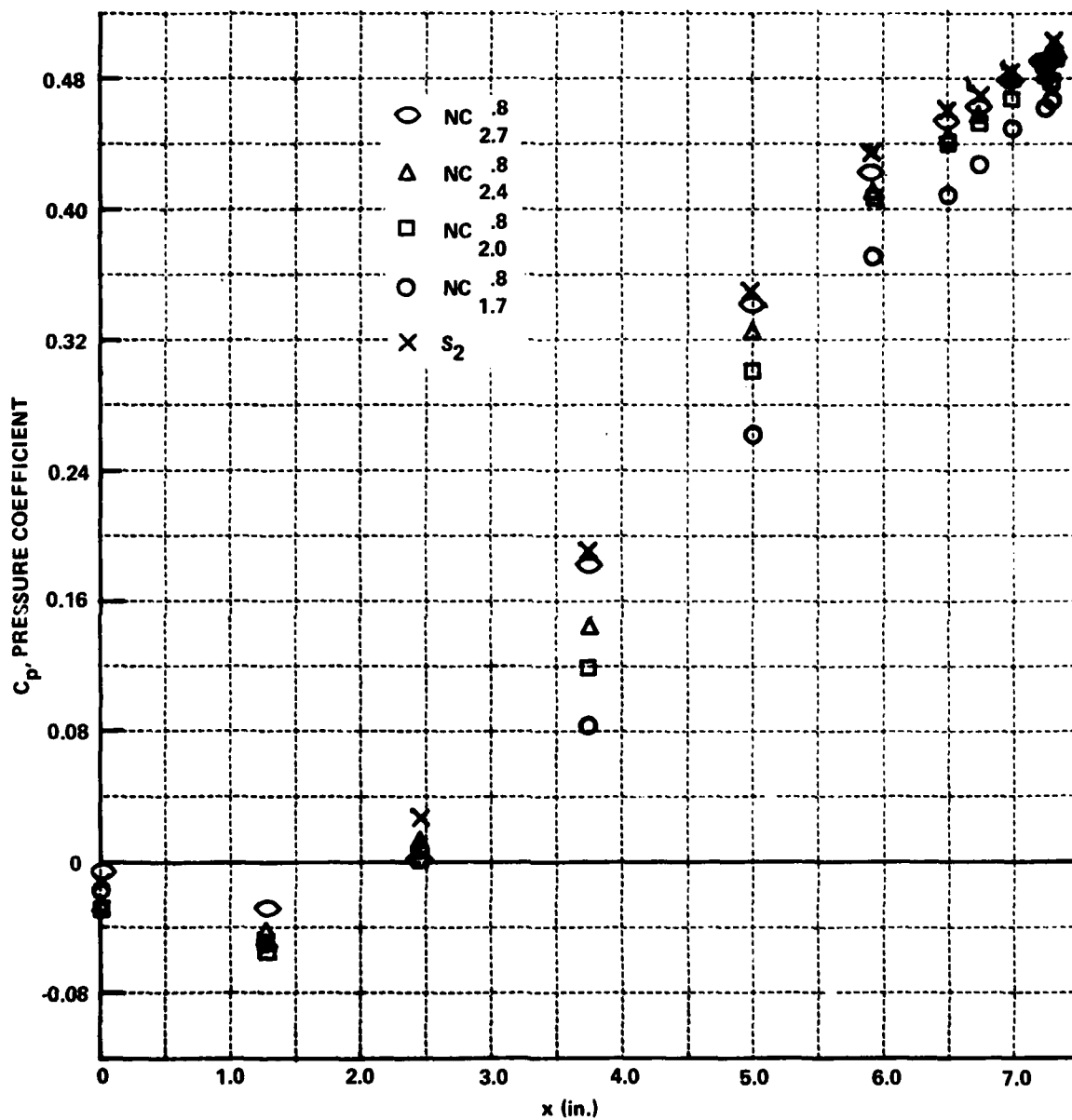


Figure 19 COMPARISON OF AFTERBODY PRESSURE DISTRIBUTIONS WITH ROCKET NOZZLES OPERATING AT DESIGN VALUES -  $M_{\infty} = 1.1$

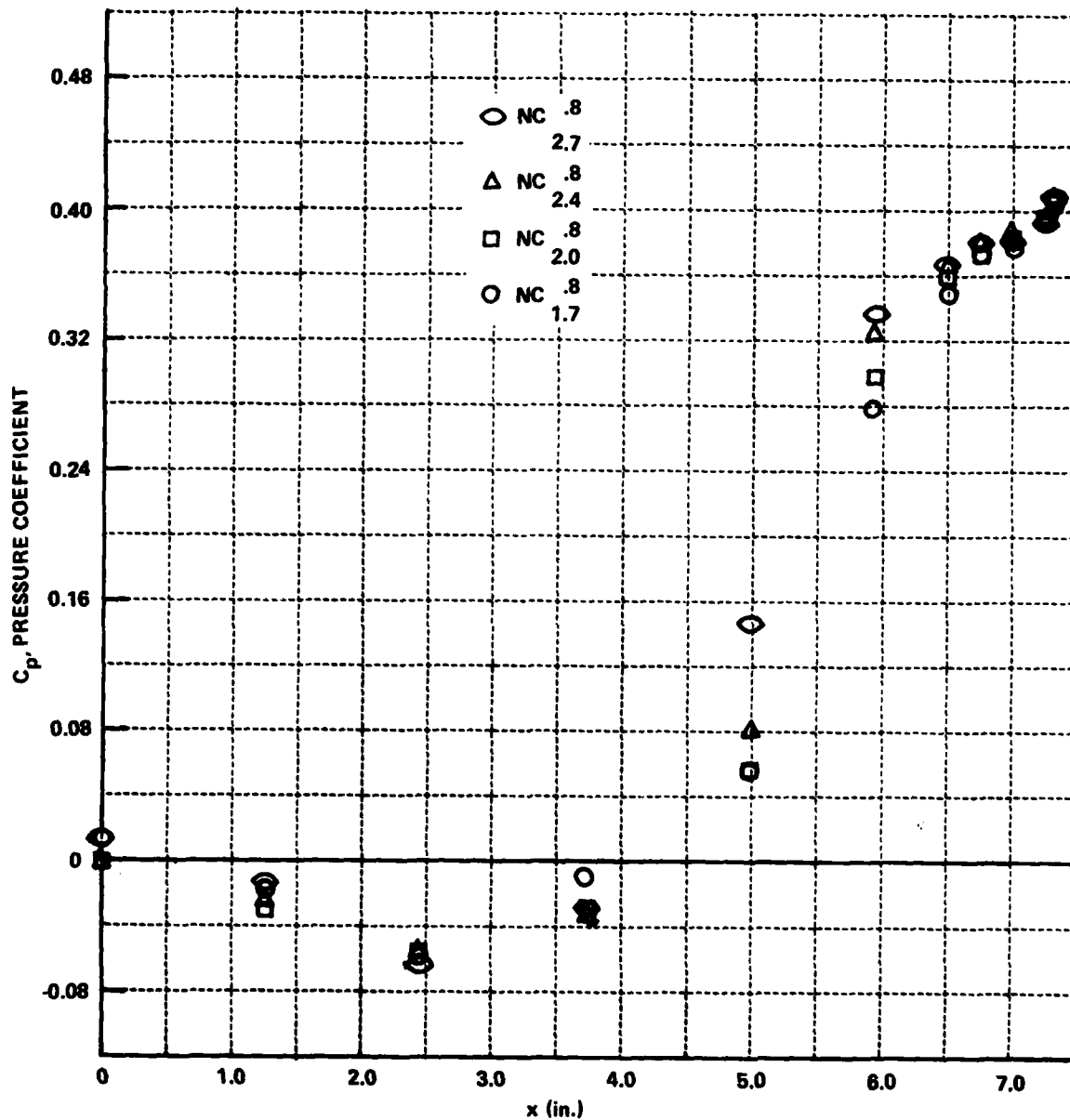


Figure 20 COMPARISON OF AFTERBODY PRESSURE DISTRIBUTIONS WITH ROCKET NOZZLES OPERATING AT DESIGN VALUES -  $M_\infty = 1.25$

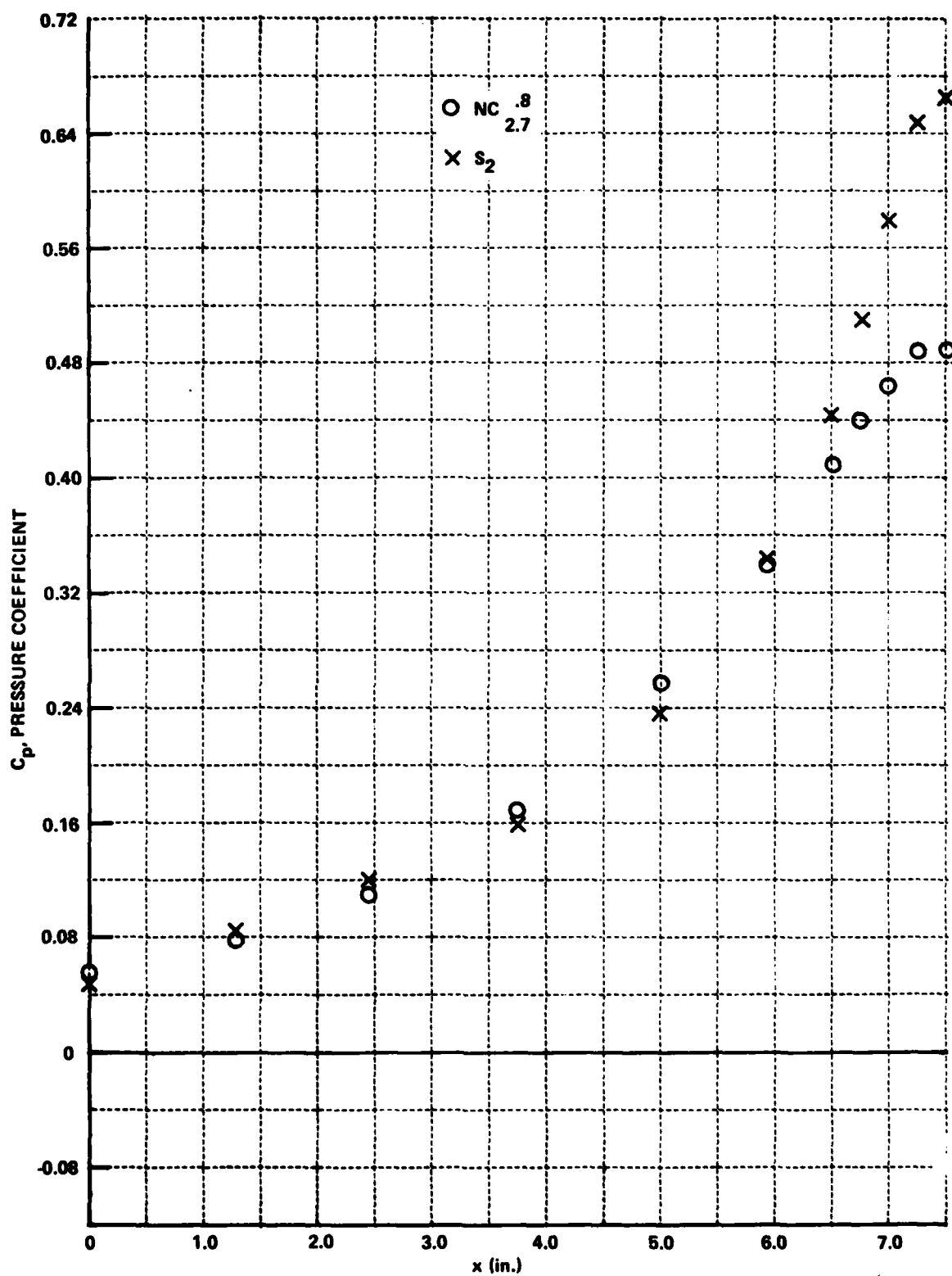


Figure 21 COMPARISON OF AFTERBODY PRESSURE DISTRIBUTIONS FOR SOLID JET SIMULATOR AND NOZZLE NC 2.7 AT DESIGN RATIO -  $M_\infty = 0.9$ ,  $\alpha = -5^\circ$

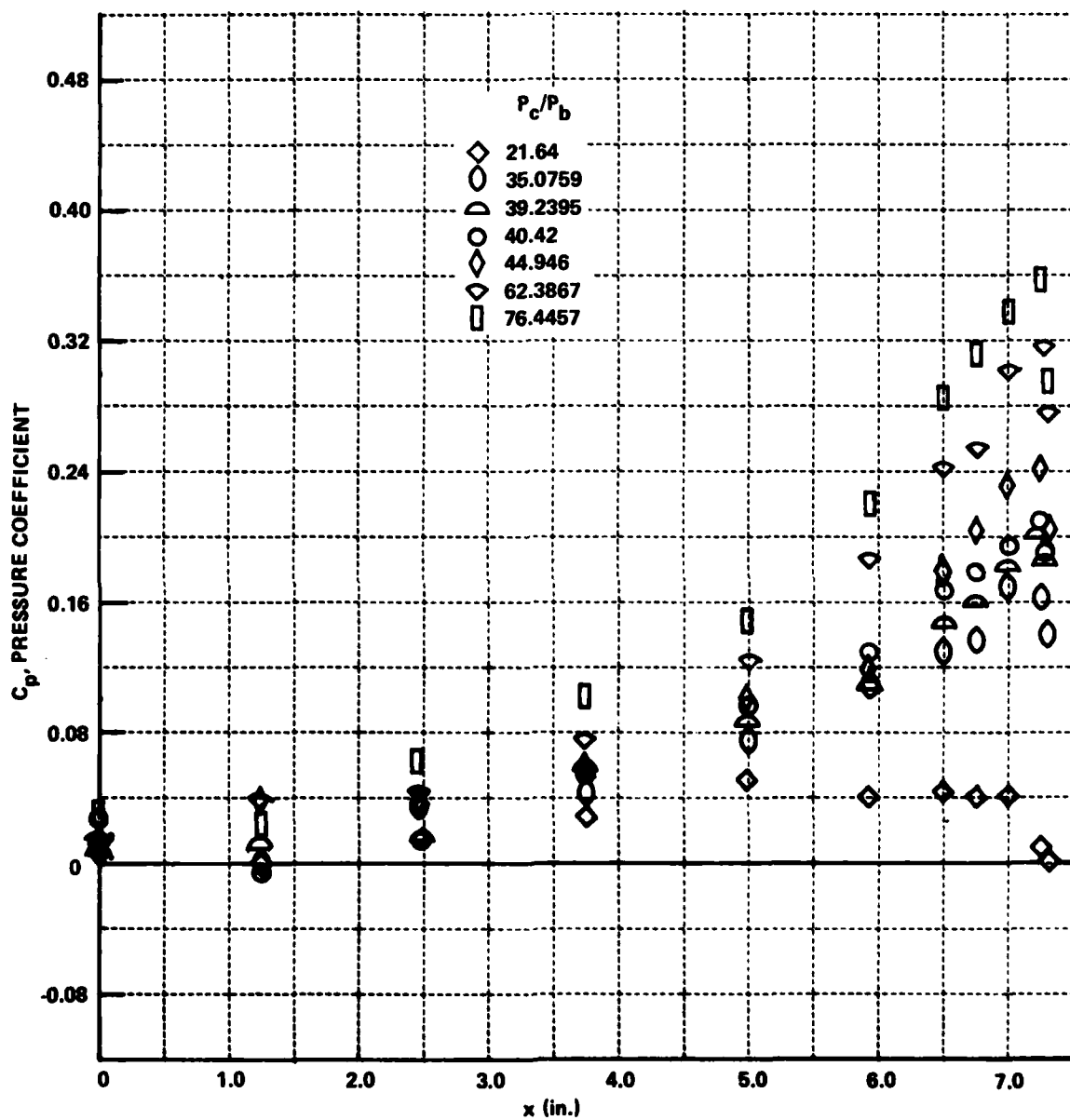


Figure 22 EFFECT OF NOZZLE TOTAL PRESSURE TO BASE PRESSURE RATIO ON AFTERBODY PRESSURE DISTRIBUTION — NC  $\frac{.8}{1.7}$ ,  $M_\infty = 0.4$

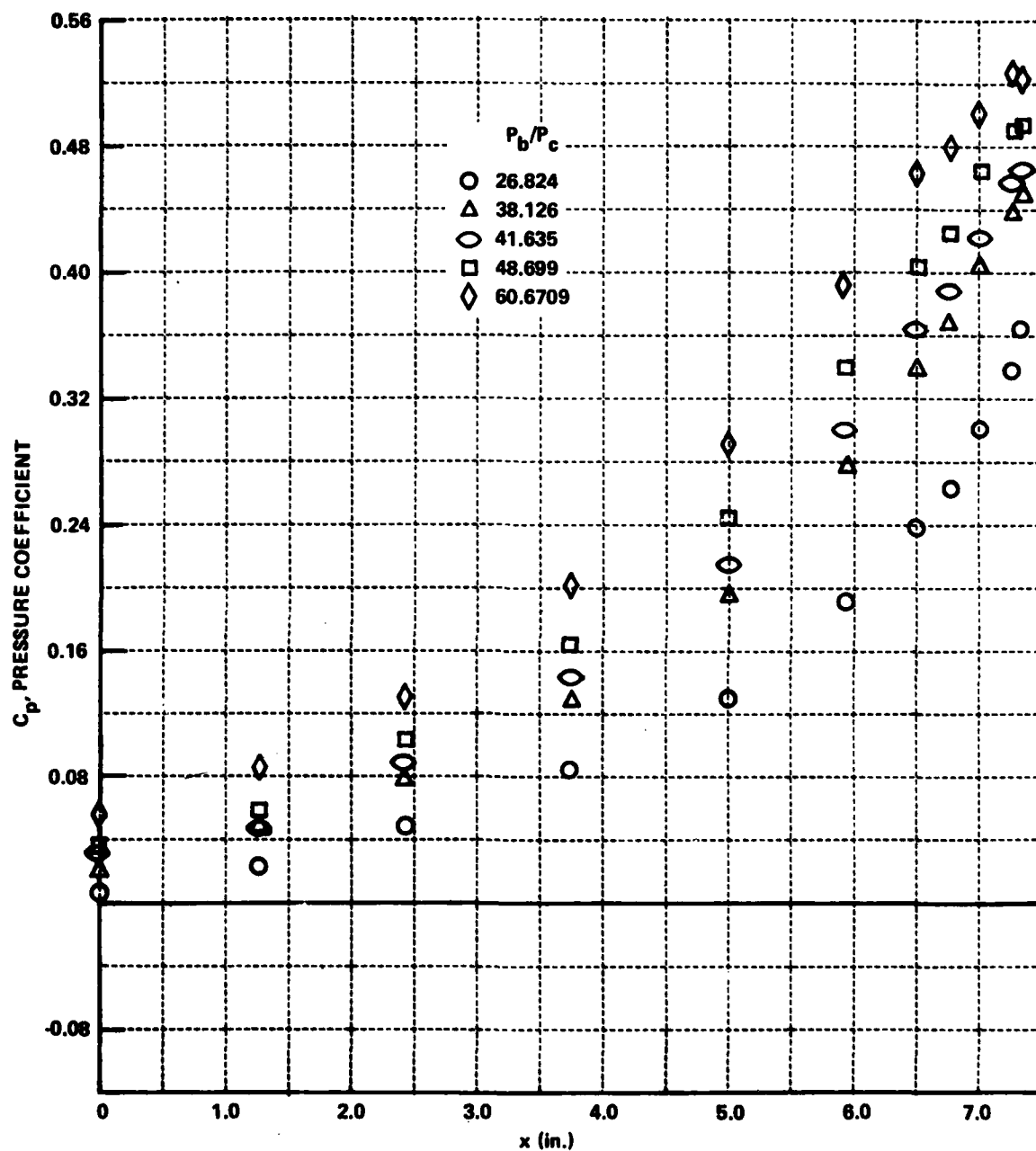


Figure 23 EFFECT OF NOZZLE TOTAL PRESSURE TO BASE PRESSURE RATIO ON AFTERBODY PRESSURE DISTRIBUTION -  $NC_{1.7}^{.8}$ ,  $M_\infty = 0.9$

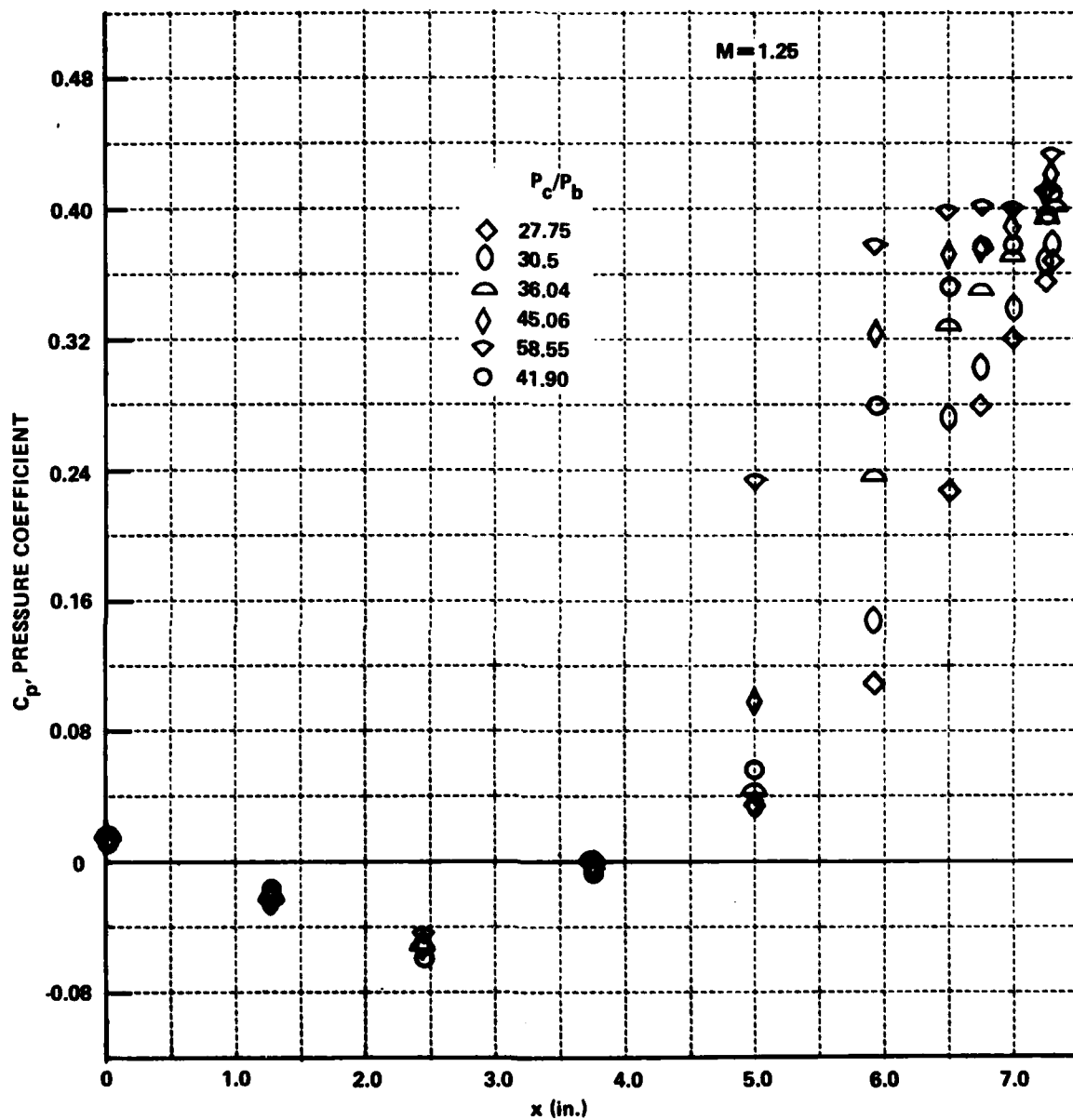


Figure 24 EFFECT OF NOZZLE TOTAL PRESSURE TO BASE PRESSURE RATIO ON AFTERBODY PRESSURE DISTRIBUTION - NC<sub>1.7</sub><sup>.8</sup>,  $M_\infty = 1.25$

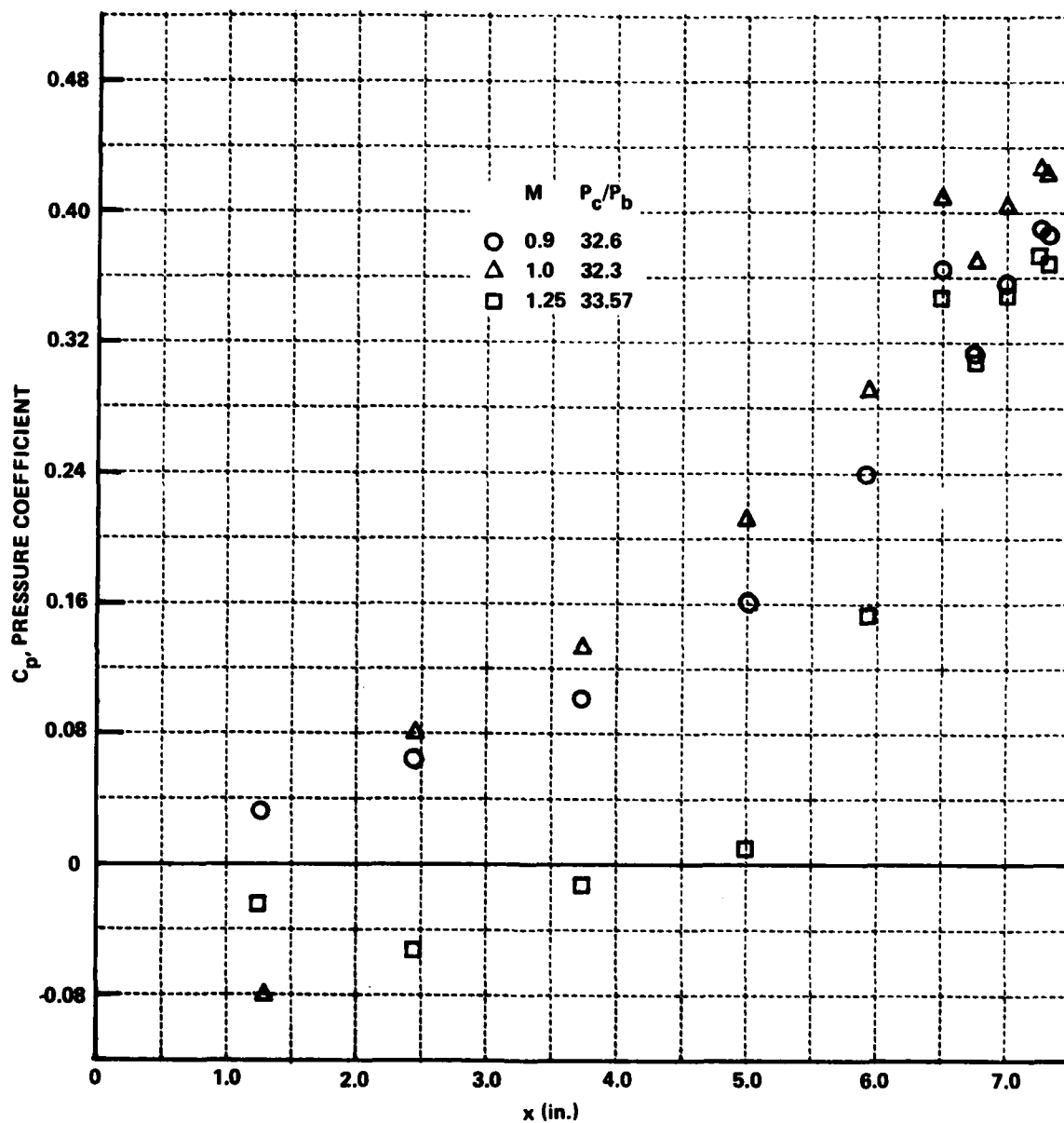


Figure 25 AFTERBODY PRESSURE DISTRIBUTION ON LARGE ZAP NOZZLE – NZ .93  
1.76

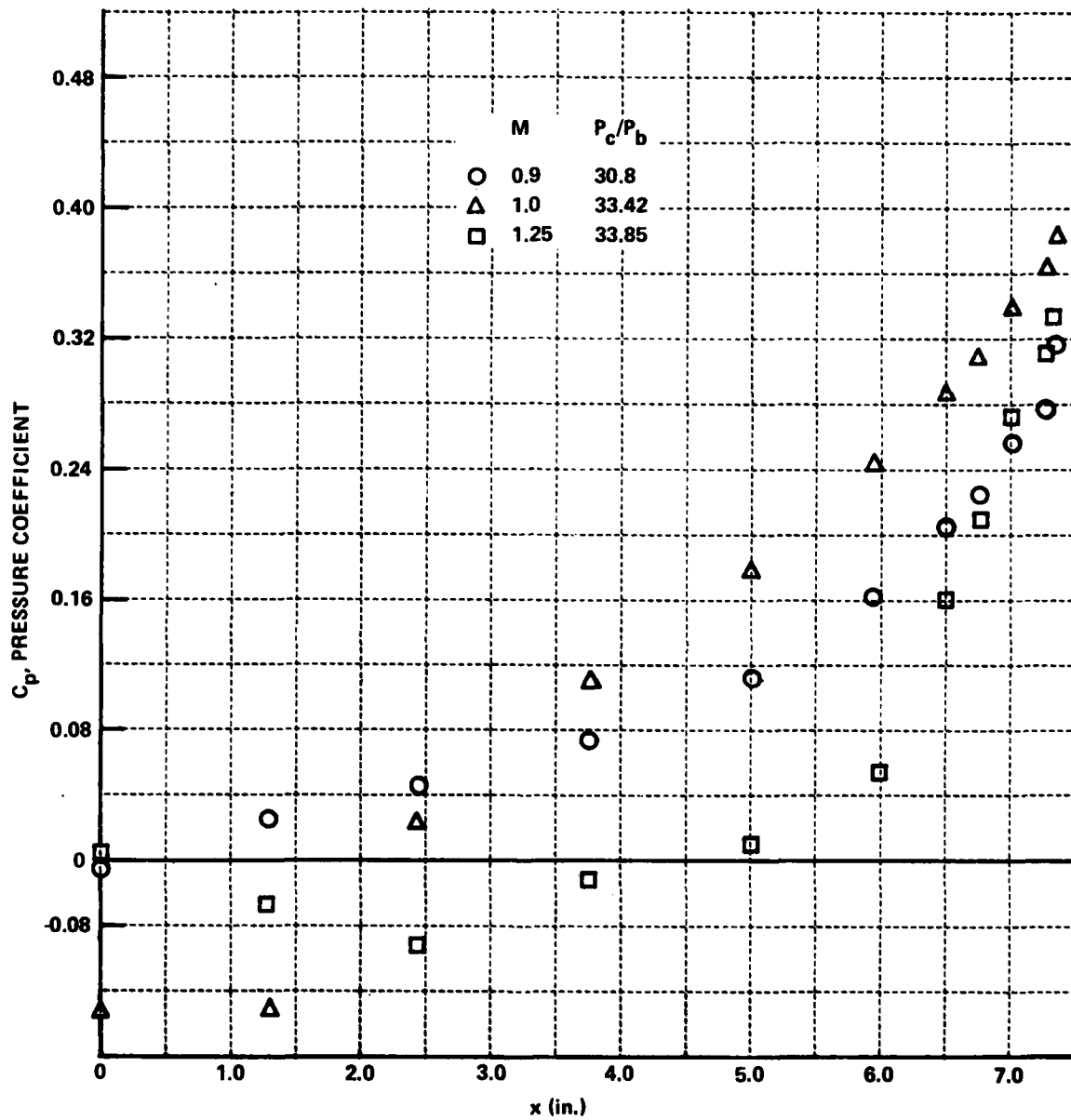


Figure 26 AFTERBODY PRESSURE DISTRIBUTION ON SMALL ZAP NOZZLE - NZ <sub>1.76</sub> .8

## REFERENCES

1. Addy, A.L. "Analysis of the Axisymmetric Base-Pressure and Base-Temperature Problem with Supersonic Interacting Freestream-Nozzle Flows based on the Flow Model of Korst, et al, Part II: A Comparison and Correlation with Experiment for Cylindrical Afterbodies," U.S. Army Missile Command, Redstone Arsenal, Alabama, Report No. RD-TR-69-13, December 1969.
2. Dash, S.M., Wilmoth, R.G. and Pergament, H.S. "Overlaid Viscous/Inviscid Model for the Prediction of Near-Field Jet Entrainment," AIAA Journal, Vol. 17, #9, pp. 950-957, September 1979.
3. Nyberg, S.E., Agrell, J. and Hering, T. "Investigation of Modeling Concepts for Plume-Afterbody Flow Interactions," Aeronautical Research Institute of Sweden Annual Report, DAERO-78-6-028, January 1978 - January 1979.
4. Korst, H.H. "Approximate Determination of Jet Contours Near the Exit of Axially Symmetrical Nozzles as a Basis for Plume Modeling," U.S. Army Missile Command Technical Report RD-72-14, August 1972.
5. Korst, H.H. and Deep, R.A. "Modeling of Plume Induced Interference Problems in Missile Aerodynamics," AIAA Paper 79-0362, January 1979.
6. Johannesen, N.H. and Meyer, R.E. "Axially-Symmetric Supersonic Flow Near the Center of an Expansion," The Aeronautical Quarterly, Vol. 2, pp. 127-142, 1950.
7. Reid, C.F. "Effects of Jet Plumes on Pressure Distributions Over a Cylindrical Afterbody at Transonic Speeds," Calspan Report No. AA-4017-W-15, February 1979.
8. Curtis, J.T., Moselle, J.R. and Marrone, P.V. "Plume Interference Prediction (PIP) Code: Users Manual and Test and Evaluation Report," Calspan Report No. KC-5900-A-6, Vol. I, April 1977.
9. May, Jr., R.J., Thompson, H.D. and Hoffman, J.D. "Comparison of Transonic Flow Solutions in C-D Nozzles," AFAPL-TR-74-110, October 1974.
10. Burke, A.F. and Bird, K.D. "The Use of Conical and Contoured Expansion Nozzles in Hypervelocity Facilities," Cornell Aero. Lab. Report No. 112, July 1962.
11. Sauer, R. "General Characteristics of the Flow Through Nozzles at Near Critical Speeds," NACA TM No. 1147, (1947).

#### REFERENCES (continued)

12. Hall, I.M. "Transonic Flow in Two-Dimensional and Axially-Symmetric Nozzles," Quarterly Journal of Mechanics and Applied Mathematics, Vol. XV, Pt. 4, pp. 487-508, (1962).
13. Kliegel, J.R. and Levine, J.N. "Transonic Flow in Small Throat Radius of Curvature Nozzles," AIAA Journal, Vol. 7, No. 7, pp. 1375-1378, July 1968.
14. Adamson, Jr., T.C. "The Structure of the Rocket Exhaust Plume Without Reaction at Various Altitudes," U. of Michigan Inst. of Science and Tech. Report of BAMIRAC 4613-45-T, June 1963.
15. Adamson, Jr., T.C. and Nicholls, J.A. "On the Structure of Jets From Highly Underexpanded Nozzles into Still Air," Journal of the Aero/Space Sciences, Vol. 26, No. 1, pp. 16-24, January 1959.